Interdisciplinary Research in Medical Sciences Specialty
ISSN: 3062-4401
2025, Volume 5, Issue 1, Page No: 212-239

Available online at: www.galaxypub.co/page/journals

Galaxy Publication

Circulating Endothelial Microvesicles Drive and Reflect Vascular Aging via miR-17-5p–Mediated Signaling

Hans Müller[1]*, Anna Schmidt[1], Thomas Weber[2]

[1]Department of Vascular Biology and Aging Research, Faculty of Medicine, University of Bonn, Bonn, Germany.
[2]Department of Extracellular Vesicles and MicroRNA Signaling, Faculty of Medicine, LMU Munich, Munich, Germany.

***E-mail** ✉ hans.mueller@uni-bonn.de

Received: 31 March 2025; **Revised:** 12 June 2025; **Accepted:** 15 June 2025

ABSTRACT

Vascular aging, defined by senescence and diminished functionality of brain endothelial cells (ECs), contributes importantly to multiple age-related cerebrovascular and neurodegenerative pathologies. Microvesicles (EMVs) and exosomes (EEXs) released by endothelial cells maintain the molecular characteristics of their parent cells and transport bioactive molecules capable of modulating recipient cell behavior. Nevertheless, the specific contributions of these vesicles to vascular aging processes remain incompletely understood. In this investigation, evaluations employing SA-β-gal staining, cerebral blood flow assessment, blood–brain barrier permeability, aging-associated molecular markers, and cognitive function testing demonstrated that EMVs secreted by young ECs provided superior attenuation of cerebrovascular and brain aging in mice compared with EEXs from the same cells. In contrast, EMVs originating from aged ECs promoted more pronounced aggravation of cerebrovascular and brain aging in mice than did EEXs released by aged ECs. Subsequent experiments established that these EMVs influence cerebrovascular and brain aging primarily through delivery of miR-17-5p and exert regulatory effects on EC senescence and activity via the miR-17-5p/PI3K/Akt signaling cascade. In older human subjects, circulating EMV abundance and EMV-associated miR-17-5p expression exhibited notable changes and displayed robust correlations with reactive oxygen species levels and vascular aging indices. Receiver operating characteristic curve analysis supported the utility of EMVs and EMV-miR-17-5p as potential diagnostic biomarkers of vascular aging. Overall, the results uncover previously unrecognized functions of EMVs, which exert more potent modulatory effects on vascular and brain aging than EEXs through control of EC behavior via the miR-17-5p/PI3K/Akt pathway. These findings further position EMVs and EMV-miR-17-5p as promising candidates for biomarkers and therapeutic intervention in vascular aging.

Keywords: Brain aging, Cerebrovascular aging, Endothelial cell functions, Endothelial exosomes (EEXs), Endothelial microvesicles (EMVs), MiR-17-5p

How to Cite This Article: Müller H, Schmidt A, Weber T. Circulating Endothelial Microvesicles Drive and Reflect Vascular Aging via miR-17-5p–Mediated Signaling. Interdiscip Res Med Sci Spec. 2025;5(1):212-39. https://doi.org/10.51847/6hOloGBwCF

Introduction

Aging together with its associated disorders constitutes one of the foremost global health and societal concerns. Estimates suggest that over 20% of the world population will exceed 60 years of age by 2050 [1]. Vascular aging is tightly intertwined with overall organismal aging and frequently leads to inadequate blood supply to organs, thereby causing tissue atrophy and functional deterioration [2]. Within the central nervous system, vascular aging accelerates brain aging, manifesting as progressive cognitive and sensorimotor deficits that may culminate in neurodegenerative conditions [3, 4]. Consequently, accurate monitoring and effective prevention of vascular aging hold considerable importance for the management of age-related pathologies, especially those impacting the brain. Currently, however, robust methods for the assessment or reversal of vascular and brain aging are insufficient.

Early vascular aging is prominently featured by endothelial cell (EC) senescence accompanied by functional compromise [1]. During this process, key EC behaviors—including proliferation, migration, responses to oxidative stress, and regulation of apoptosis—become disordered [5], while senescent ECs progressively accumulate [1]. These alterations heighten vascular susceptibility and foster the development of disorders such as neurodegenerative decline, atherosclerosis, and cerebrovascular pathology [1, 6]. Oxidative stress and apoptotic pathways represent central, mutually reinforcing components of the cellular senescence program [7, 8]. In light of these observations, ECs emerge as valuable cellular targets for both evaluation and therapeutic modulation of vascular aging. Extracellular vesicles, encompassing mainly microvesicles and exosomes, are liberated by multiple cell types in response to various stimuli or apoptotic cues [9, 10]. Such vesicles conserve molecular traits of their cells of origin and mediate diverse effects on target cells by shuttling intracellular constituents [11]. Endothelial microvesicles (EMVs) and endothelial exosomes (EEXs) function as significant vehicles for intercellular signaling [12] and may additionally serve as innovative indicators of endothelial dysfunction or injury [9, 11]. The generation and physiological actions of EMVs and EEXs are strongly influenced by the activation status and overall condition of the source ECs. Under homeostatic conditions, EMVs and EEXs support viability and restrain apoptotic activity in human brain ECs [13, 14]. By comparison, EMVs induced by hyperglycemia or EEXs generated under atheroprone low-oscillatory shear stress have been found to elevate apoptosis rates in human umbilical vein ECs (HUVECs) [15, 16]. Plasma concentrations of EMVs rise substantially among elderly individuals [17]. An earlier report showed that administration of young mouse blood mitigated cognitive deficits and synaptic plasticity impairments associated with senescence in aged animals [18], raising the possibility that young EEXs or EMVs could offer a novel acellular strategy for counteracting aging. Of note, the mechanisms governing the formation of EMVs differ from those of EEXs, and their respective impacts on recipient cells and tissues have not been systematically compared [9, 11]. Drawing upon these insights, we postulated that EMVs and EEXs may exert pivotal influences on cerebrovascular and brain aging, EC functionality, and could additionally qualify as useful biomarkers for vascular aging.

MicroRNAs (miRNAs) act as critical regulators of cellular senescence and multiple cellular processes, constituting the predominant functional payload within EMVs and EEXs. As one illustration, EMV levels harboring miR-126 decline markedly in individuals with diabetes mellitus [19]. EMVs enriched with miR-126 stimulate migration and proliferation in human coronary artery ECs [19]. Likewise, miR-19a-3p delivered by HUVEC-derived EEXs augments endothelial tube formation and proliferative capacity [20]. Hence, the identification of specific miRNAs responsible for mediating EMV- and EEX-dependent regulation of vascular aging warrants detailed examination.

The current work seeks to delineate the therapeutic capacities and differential attributes of EMVs versus EEXs in the control of cerebrovascular and brain aging. Particular attention is devoted to clarifying the miRNA-based mechanisms involved and evaluating biomarker potential. We first examined the consequences of EMVs and EEXs isolated from young versus aged mouse brain ECs upon cerebrovascular and brain aging parameters. Upon determining that EMVs produced stronger effects than EEXs, we proceeded to characterize EMV actions on EC performance in both living organisms and cultured systems, pinpointed miR-17-5p as the major functional miRNA constituent within EMVs, and interrogated the pertinent downstream pathways to uncover the mechanistic basis. Complementing these preclinical studies, clinical analyses quantified plasma EMV levels and associated miRNAs in individuals across age ranges to assess linkages with vascular aging.

Materials and Methods

Animal and ethics

Every procedure performed on animals strictly followed the ARRIVE reporting guidelines and the directives of the National Institutes of Health Guide for the Care and Use of Laboratory Animals. Prior ethical clearance was granted by the Institutional Animal Care and Use Committee of Guangdong Medical University under approval number GDY1902103.

Isolation and culture of primary mouse brain microvascular endothelial cells

Primary brain microvascular endothelial cells (BMECs) were derived from 2-week-old C57BL/6 mice following established isolation techniques [21]. Cells were initially plated at 1.0 × 10^4 cells/cm² and allowed to grow to near-confluence (90%) before being passaged. Passaging involved treatment with trypsin-EDTA (Gibco, cat#

25200072). Confirmation of endothelial identity relied on immunofluorescence labeling for CD31 (1:500, CST, USA, cat# 3528S) and CD34 (1:300, abcam, cat# ab229021). The degree of senescence in these cultures was monitored using senescence-associated β-galactosidase (SA-β-gal) activity. Young BMECs were defined as those maintained through early passages (P 2–4) displaying less than 5% SA-β-gal positivity, whereas old BMECs corresponded to later passages (P 15–16) showing more than 60% SA-β-gal positivity [22, 23].

Preparation, analysis and characterization of EMVs and EEXs

EMVs and EEXs were separated through sequential ultracentrifugation steps. Supernatants collected from cultures of young BMECs (y.cells) and old BMECs (o.cells) first underwent centrifugation at 300 rcf for 15 min and then at 2000 rcf for 20 min to clear debris. The clarified liquid was spun at 20,000 rcf for 70 min to harvest the EMV population (y.EMVs from young cells and o.EMVs from old cells). The post-EMV supernatants received further ultracentrifugation at 100,000 rcf for 2 h to isolate EEXs (y.EEXs and o.EEXs). Vesicle concentrations were quantified after 1/200 dilution in PBS with the NTANS300 Instrument (Malvern Instruments, United Kingdom) in light-scatter configuration using a 405-nm laser; each measurement consisted of three 30-second videos captured at 30 frames per second. Morphological features and size profiles of the isolated vesicles were examined by transmission electron microscopy (TEM) according to methods described earlier [24]. All preparations were kept at −80°C until needed to preserve bioactivity. Quantification of EMVs and EEXs was conducted by personnel blinded to the experimental groups.

Incorporation study of EMVs and EEXs in vitro and in vivo

Quantities of 1 × 10^9 EMVs or EEXs were first labeled with PKH 26 fluorescent dye (2 μM, Sigma, USA, cat# PKH26GL) [25]. After labeling, the vesicles were resuspended in PBS and introduced either to cultured BMECs or administered systemically to mice [26]. Uptake efficiency was assessed via confocal microscopy (OLYMPUS, FV3000, Japan), with all conditions performed in triplicate.

Animals, sample size calculation and grouping

C57BL/6 mice (30 males and 30 females) were acquired from the Nanjing Biomedicine Institute of Nanjing University and maintained in a controlled facility with continuous access to standard diet and water. Mice aged 3 months served as the young cohort (y.mice), while 24-month-old animals represented the old cohort (o.mice). After initial tests revealed minimal impact of y.EEXs/y.EMVs and o.EEXs/o.EMVs on cerebrovascular features in both age groups, the study shifted focus to evaluating o.EEXs/o.EMVs in y.mice and y.EEXs/y.EMVs in o.mice. Random assignment placed animals into six groups of 10 mice each: y.mice + saline, y.mice + o.EMVs, y.mice + o.EEXs, o.mice + saline, o.mice + y.EMVs, and o.mice + y.EEXs. Treatments consisted of tail-vein delivery of 1 × 10^10 EMVs or EEXs in 100 μL 0.9% saline (or saline vehicle alone) once per week across five consecutive weeks.

Biodistribution of EMVs in mice

Distribution patterns of EMVs in living mice were tracked after labeling with the fluorescent membrane dye DiR (1,1-dioctadecyl-3,3,3,3-tetramethylindotricarbocyanine iodide) (Yeasen Biotechnology, cat# 40757ES25) and imaging on a Bruker in vivo Xtreme platform (USA). Labeling involved incubating EMVs with 5 μM DiR for 20 min at room temperature in darkness, followed by centrifugation at 20,000 rcf for 70 min. The collected pellet was resuspended in 100 μL PBS for intravenous injection. Control animals received the supernatant from the final wash step to exclude contributions from free dye. Imaging sessions occurred on isoflurane-anesthetized live animals or on harvested organs after euthanasia. Signal acquisition lasted 12 s (excitation 748 nm, emission 780 nm) on a Carestream MI system, with intensity reported in relative fluorescence units (RFU) [27].

Morris water maze test

Evaluation of learning and memory capabilities relied on the Morris water maze assay conducted according to standardized methods [28]. Measured variables encompassed duration spent in the target quadrant, platform crossing frequency at the original location, and overall search strategy.

Cerebral blood flow and blood brain barrier function measurements

Laser speckle contrast imaging with the PeriCam PSI System (Perimed, Sweden) served to quantify cerebral blood flow (CBF) in accordance with established protocols [29]. Animals were anesthetized with isoflurane (2%–2.5% in a mixture of 70% N_2O and 30% O_2) and fixed in a stereotaxic apparatus. Following a midline scalp incision to expose the skull, continuous imaging of the intact cranium was carried out for 60 s, after which perfusion parameters were processed using Pimsoft software.

Assessment of blood-brain barrier (BBB) disruption relied on Evans blue (EB) extravasation following exposure to various EMV or EEX preparations, consistent with prior methodologies [30]. Absorbance measurements were converted to EB content via a standard curve, with final concentrations reported as μg/g tissue.

Detection of aging associated biomarkers

Key aging-related markers such as MDA, GSSG, and Klotho were quantified using commercial assay kits according to the suppliers' instructions (MDA: Beyotime, cat# S0131M; GSSG: Beyotime, cat# S0053; Klotho: ZCI Bio, cat# ZC-31968) as previously detailed [31-33]. TERT mRNA levels were determined through quantitative PCR. Experiments were conducted in triplicate.

SA-β-gal staining in mice hippocampus and basilar artery

In line with earlier recommendations [34, 35], cerebrovascular aging was evaluated by SA-β-gal staining of the basilar artery. Brain tissues were processed as reported previously [29]: specimens were placed in PBS within a 10 cm Petri dish, the brainstem was isolated and oriented vertically in O.C.T. embedding medium (Solarbio, China), and 20 μm coronal cryosections were generated. SA-β-gal enzymatic activity was detected following the manufacturer's guidelines [24]. The percentage of SA-β-gal-positive (blue-stained) cells relative to total cells was calculated in the basilar artery and hippocampal CA3 region using Image J software (NIH). Counts were obtained from five randomly chosen microscopic fields per animal across six mice per group.

Immunofluorescent staining of mouse brain slices

Coronal brain sections of 20 μm thickness were prepared with a cryostat as described in prior work [25, 29]. Microvascular density and the colocalization of ROS/NO production and apoptosis with endothelial cells were examined in the hippocampus. Sections were incubated overnight at 4°C with anti-CD31 mouse monoclonal antibody (1:500, CST, USA, cat# 3528S), followed by goat anti-mouse IgG H&L conjugated to Alexa Fluor® 647 (1:500, Abcam, cat# ab150115) for 60 min. CD31-labeled microvascular structures were imaged using an OLYMPUS FV3000 fluorescence microscope.

Sequential staining was employed to evaluate ROS, NO, and apoptosis within brain endothelial cells. ROS and NO levels were detected by incubation with DCFH-DA (10 μM, Beyotime, #S0033S) or DAF-FM DA (5 μM, Beyotime, #S0019) for 30 min at 37°C in the dark. Apoptosis was visualized with TUNEL assay (Beyotime, #C1086) for 60 min at 37°C protected from light. Nuclei were stained with DAPI (1 μM, Beyotime, #C1006) for 10 min at room temperature. Fluorescence was acquired at 488 nm for DCFH-DA and TUNEL signals, and at 495 nm for DAF-FM DA, under uniform microscope settings. Positive cell ratios were determined from five random fields per section. Three consecutive rostrocaudal sections were analyzed per mouse, and average values were computed for each subject. Image acquisition utilized FV31S-SW software (Ver 2.3.1), while quantification was performed with Image J (NIH). All image analyses were carried out by personnel blinded to experimental conditions.

Analysis of miR-17-5p level in mice brain

Cortical tissue (100 mg) was harvested from the left hemisphere of each mouse and homogenized. Total RNA was isolated using TRIzol reagent (Invitrogen, Carlsbad, CA). RNA integrity was confirmed by spectrophotometry (OD260/OD280 ratio of 1.7–2.0). Relative expression of miR-17-5p was measured with the Hairpin-it™ miRNA RT-PCR Quantitation Kit (GenePharma, Shanghai, China) on a Roche LightCycler 480 Instrument II (Roche), employing the protocol outlined above.

MiRNA sequencing

Total RNA extracted from y.EMVs and o.EMVs using the miRNeasy Kit (Qiagen Inc., Valencia, CA, USA) served as input material. RNA concentration and quality were assessed with a Qubit 3.0 Fluorometer (Invitrogen) and Agilent 2100 Bioanalyzer (Applied Biosystems). Small RNA sequencing libraries were generated from 100

ng RNA with the VAHTS™ Small RNA Library Prep Kit for Illumina® (Vazyme Biotech) [36]. Known miRNAs were annotated against miRBase v22 using the exceRpt pipeline, and novel miRNAs were predicted by miRDeep2. Expression values were normalized via the TMM algorithm, and differential expression was analyzed with edgeR. Transcripts meeting the criteria of $p < 0.05$ and fold change ≥ 1.5 were classified as differentially expressed.

MiR-17-5p regulatory network analyzed by ingenuity pathway analysis

Ingenuity Pathway Analysis (IPA; Ingenuity Systems, Mountain View, CA, USA) was applied to construct the miR-17-5p regulatory network [37]. Differentially expressed genes were integrated into established biological pathways and interaction networks using rodent and human ortholog mappings. Network prioritization relied on scores generated from the Ingenuity Knowledge Base, with original datasets deposited in Data S1. Statistical threshold was set at $p < 0.05$. Informed by IPA outcomes, y.cells were pretreated with the PI3K activator 740Y-P (10 μM; Selleckchem) and o.cells with the PI3K inhibitor LY294002 (20 μM; Selleckchem) for 2 h prior to initiating in vitro functional assays.

Luciferase reporter assays

The PI3K coding sequence was amplified by PCR from genomic DNA and cloned downstream of the luciferase reporter gene in the pGL-3 control vector (Clontech). HBMECs were plated in 24-well plates and grown for 24 h before transfection with 200 ng of reporter plasmid plus Renilla luciferase control plasmid using Lipofectamine 3000 (Invitrogen). To test miR-17-5p effects, 20 μM synthetic miRNA mimics were co-transfected. Cells were lysed 48 h after transfection, and luciferase activity was determined with the Dual-Luciferase Reporter Assay System (Promega, USA). Firefly luciferase values were normalized to Renilla luciferase activity within each sample. Data represent the mean ± SEM of three independent replicates.

Detection of EMVs carrying miR-17-5p

Visualization of miR-17-5p contained inside EMVs after uptake by target cells and within the mouse hippocampus was achieved using a FAM-conjugated peptide nucleic acid (PNA) probe specifically designed for miR-17-5p (FAM-miR-17-5p). BMECs were transfected employing Lipofectamine 3000 (Invitrogen, California, USA) as instructed by the manufacturer. EMVs harboring FAM-miR-17-5p (EMVs-FAM-miR-17-5p) were subsequently harvested from the transfected BMECs and labeled with PKH 26 dye (2 μM, Sigma, USA, cat# PKH26GL). The presence and distribution of these miR-17-5p-carrying EMVs in BMECs and mouse hippocampal regions were observed by fluorescence microscopy (OLYMPUS, FV3000, Japan) [38].

RNA extraction and quantitative reverse transcription PCR (RT-PCR)

Quantification of miR-17-5p expression levels in y.EMVs/o.EMVs, cultured BMECs, and mouse brain tissue was performed by RT-PCR following previously validated laboratory procedures [24].

MiR-17-5p overexpression and knockdown in BMECs and the grouping of experiments

Lentiviral transduction was used to generate BMEC lines with stable overexpression or knockdown of miR-17-5p [29]. Lentiviral constructs expressing GFP-tagged miR-17-5p mimic (Lv-miR-17-5p), miR-17-5p-specific shRNA (Lv-si-miR-17-5p), or matched scrambled controls (Lv-SC) were supplied by GenePharma Biotech (Shanghai, China). Old cells (o.cells) at 75% confluence in 6-well plates were transduced with 1×10^7 infectious units of Lv-miR-17-5p or Lv-miR-17-5pSC. Young cells (y.cells) received 1×10^7 infectious units of Lv-si-miR-17-5p or Lv-si-miR-17-5pSC, resulting in the cell lines o.cells$^{miR\text{-}17}$, o.cells$^{miR\text{-}17SC}$, y.cells$^{miR\text{-}17KO}$, y.cells$^{miR\text{-}17KOSC}$ [29]. After 24 h, conditioned media from these cultures were collected to isolate the corresponding EMVs: o.EMVs$^{miR\text{-}17}$, o.EMVs$^{miR\text{-}17SC}$, y.EMVs$^{miR\text{-}17KO}$, and y.EMVs$^{miR\text{-}17KOSC}$. Successful transduction was confirmed under fluorescence microscopy. miR-17-5p abundance in the modified cells and vesicles was validated by RT-PCR [29] with U6 serving as the reference gene. All reactions were run in triplicate, and relative expression was calculated using the $2^{-\triangle\triangle Ct}$ method. These engineered EMVs were then applied in functional studies involving animals and BMECs. The experimental groups consisted of: y.mice/y.cells, y.mice/y.cells + o.EMVs, y.mice/y.cells + o.EMVs$^{miR\text{-}17SC}$, y.mice/y.cells + o.EMVs$^{miR\text{-}17}$, o.mice/o.cells, o.mice/o.cells + y.EMVs, o.mice/o.cells + y.EMVs$^{miR\text{-}17KOSC}$, o.mice/o.cells + y.EMVs$^{miR\text{-}17KO}$. Assessments of cerebrovascular and brain aging in animals were conducted as outlined earlier.

Endothelium-specific overexpression and knockout of miR-17-5p

To examine the contribution of miR-17-5p to the control of cerebrovascular and brain aging, endothelium-targeted modulation was implemented. Adeno-associated virus serotype 9 (AAV9) vectors expressing miR-17-5p driven by the endothelial-specific TIE promoter (TIEmiR-17-5p AAV9) were generated. AAV9 vectors carrying miR-17-5p (miR-17-5p-AAV9) or control constructs (CTL-AAV9) from Genechem (Shanghai, China) were injected stereotactically at 2 μL virus genomes per mouse [29].

Analysis of BMECs senescence and functions

BMECs grown to 75% confluence in 6-well or 96-well plates were treated with various EMV preparations (1 × 10^9 particles/mL) for 24 h before functional testing [26]. Senescence status was determined by SA-β-gal staining. Cells from passages 2–4 (P 2–4) with SA-β-gal positivity below 5% were considered y.cells, while those from passages 15–16 (P 15–16) exceeding 60% positivity were classified as o.cells [23]. Parameters including ROS/NO generation, apoptosis rate, cell migration, proliferation, and angiogenic tube formation were evaluated using previously reported techniques [29, 39].

Western blot analysis

Equal amounts of total protein (25 μg) were separated on 12% SDS-PAGE gels and transferred to PVDF membranes (0.22 μm, Millipore). After blocking with 5% skim milk for 1 h, membranes were probed overnight at 4°C with primary antibodies targeting β-actin (1:1000, Abcam, cat# ab8226), GAPDH (1:1000, Abcam, cat# ab8245), Annexin V (1:1000, Abcam, cat# ab313581), TSG101 (1:1000, Abcam, cat# ab125011), CD9 (1:1000, Abcam, cat# ab236630), CD63 (1:1000, Abcam, cat#134045), CD81 (1:1000, Abcam, cat#79559), P21 (1:1000, Abcam, cat#109520), P16 (1:1000, CST, cat#80772), P53 (1:1000, CST, cat#9282), PI3K (1:1000, CST, USA, cat# 4249S), phospho-PI3K (1:1000, CST, USA, cat# 17366S), Akt (1:1000, CST, USA, cat# 4685S), and phospho-Akt (1:1000, CST, USA, cat# 4060S). Incubation with goat anti-rabbit IgG H&L secondary antibody (1:5000, Abcam, cat# ab6721) followed [29]. Chemiluminescent detection was performed on an Azure C600 system (Azure Biosystems, USA). Band densities were quantified using Image J software (NIH) and normalized against β-actin. Statistical evaluation was conducted with GraphPad Prism 5.

Telomere length measurement

Telomere length assessment employed a monochrome multiplex quantitative PCR (MM-qPCR) approach as previously established [40]. Genomic DNA was purified from endothelial cells with the DNeasy Blood and Tissue Kit (Cat. No. 69504, Qiagen, Hilden, Germany) and diluted to 100 ng/μL in Tris-HCl (10 mmol/L, pH 7.5) containing 0.1 mmol/L EDTA. Each reaction contained 5 ng of genomic DNA. Telomere sequences were amplified using primers Telg: 5′-ACACTAAGGTTTGGGTTTGGGTTTGGGTTTGGGTTAGTGT-3′ and Telc: 5′-TGTTAGGTATCCCTATCCCTATCCCTATCCCTATCCCTAACA-3′. Normalization to the single-copy β-globin gene was achieved at 88°C with primers hbgu: 5′-CGGCGGCGGGCGGCCGGGGCTGGGCGGCTTCATCCACGTTCACCTTG-3′ and hbgd: 5′-GCCCGGCCCGCCGCGCCCGTCCCGCCGGAGGAGAAGTCTGCCGTT-3′. Telomere length was calculated as the T/S ratio (telomere to β-globin copy numbers).

Enrollment of participants and sample size calculation

Study participants were recruited at the Affiliated Hospital of Guangdong Medical University during the period spanning January 2019 to December 2020. All individuals provided written informed consent before joining the study. Inclusion criteria specified: (1) adults of either sex aged over 18 years; (2) subjects appearing healthy upon standard physical examination. Participants were excluded if they met any of the following conditions: (1) presence of established cardiovascular conditions including coronary artery disease, congestive heart failure, hypertension (blood pressure ≥140/90 mmHg), peripheral arterial disease, or prior stroke; concurrent systemic diseases such as diabetes mellitus (fasting glucose ≥7.0 mM), chronic kidney disease, chronic obstructive pulmonary disease, osteoporosis, neurological or psychiatric disorders (for example, dementia or major depressive disorder), or active cancer; (2) current pregnancy or breastfeeding. Altogether, 119 volunteers were enrolled and divided into three age-based cohorts: young adults (18–45 years, n = 58), middle-aged adults (46–65 years, n = 33), and older adults (>65 years, n = 28) [41, 42].

Intima-media thickness measurement

Measurement of carotid intima-media thickness (IMT) was conducted by B-mode ultrasound. Participants were positioned supine with 45° head elevation and 30° lateral tilt, first to the right side and subsequently to the left, with the average value recorded [43]. Each assessment was repeated three times by the same trained operator who remained unaware of the subjects' clinical status and group assignment. Vascular aging was defined as IMT values greater than 0.58 mm [1, 44-46].

Analysis of the plasma ROS level

Levels of reactive oxygen species (ROS) in plasma were determined using the DCF ROS/RNS Assay Kit (Abcam, ab238535) in accordance with the provided protocol. Blood samples were centrifuged at 10,000 rcf for 5 min, and the supernatant was mixed with DCFH solution for incubation lasting 30 min at room temperature while protected from light. Fluorescence readings were obtained on a BioTek microplate reader with excitation at 480 nm and emission at 530 nm. Plasma ROS concentrations were interpolated from a standard curve [29].

Analysis of the levels of EMVs and miR-17-5p in EMVs from plasma

Isolation of EMVs from plasma samples was achieved with commercially available kits (Life Technologies and Miltenyi Biotec) using methods described earlier [24].

Quantification of miR-17-5p within plasma-derived EMVs involved extraction of miRNA using TRIzol reagent (Invitrogen, Carlsbad, CA) combined with the miRNeasy Mini Kit according to manufacturer recommendations. The analytical steps were as follows: isolation of 20 μg total RNA with TRIzol®; synthesis of cDNA via the Hairpin-it™ miRNA RT-PCR Kit (GenePharma); and subsequent qPCR amplification employing U6 snRNA as the endogenous reference. All reactions were performed in triplicate. Relative expression of EMV-miR-17-5p was computed using the $2^{-\triangle\triangle Ct}$ formula.

Statistical analysis

Data processing and statistical evaluations were carried out with SPSS version 22.0 and GraphPad Prism 5 software. The D'Agostino-Pearson omnibus test served to evaluate normality. Two-group comparisons for normally distributed variables utilized Student's t-test. Analyses involving more than two groups employed one-way or two-way ANOVA. Relationships among parameters were explored using Spearman rank correlation. Adjusted odds ratios (ORs) with 95% confidence intervals (CI) were reported for multivariate findings. The ability of EMVs, EMV-miR-17-5p, and their combined use to discriminate vascular aging was assessed by receiver operating characteristic (ROC) curves and corresponding area under the curve (AUC) values. Results are reported as mean ± SEM. Significance levels are indicated as: ns (not significant), * ($p < 0.05$), ** ($p < 0.01$), and *** ($p < 0.001$). Throughout the study, 'n' denotes the number of mice in preclinical experiments or the number of recruited participants in the clinical component.

Results and Discussion

Determination of BMECs and the characteristics of EMVs and EEXs

Purity of isolated primary brain microvascular endothelial cells (BMECs) was established by positive immunostaining for the endothelial-specific markers CD31 (red fluorescence) and CD34 (green fluorescence). Immunofluorescence imaging confirmed successful isolation and maintenance of these primary BMECs in culture. BMECs at passages 2–4 (P 2–4) and passages 15–16 (P 15–16) were classified as y.cells and o.cells, respectively, and differentiated on the basis of SA-β-gal staining. Western blot analysis verified the enrichment of exosome-associated proteins TSG101, CD9, CD63, and CD81 in purified EEXs, whereas the microvesicle marker Annexin V was present in EMV preparations. Transmission electron microscopy (TEM) illustrated clear differences in vesicle dimensions, with EMVs ranging from 100–600 nm and EEXs from 30–100 nm. These size distributions align with previous TEM-based characterizations of EMVs and EEXs [47]. Size measurements obtained through TEM imaging were further corroborated by nanoparticle tracking analysis.

Y.EMVs mitigated and o.EMVs exacerbated cerebrovascular and brain aging more significantly than y.EEXs and o.EEXs

To assess the capacity of EMVs and EEXs for internalization within the mouse brain vasculature, PKH26-labeled vesicles were introduced via tail vein injection. PKH26, a lipophilic fluorescent dye routinely utilized for vesicle labeling [48], allowed visualization of uptake.

For comprehensive biodistribution analysis, DiR-labeled EMVs and EEXs were similarly injected [27]. Strong fluorescent signals emerged across multiple organs, including the brain, liver, lung, heart, kidney, and spleen. EMV accumulation in the brain reached its maximum between 1 and 4 h, remained visible at 8 h, and declined markedly by 24 h. Beyond 8 h, EMVs predominantly localized to the liver, persisting through 24 h. EEXs, however, showed primary distribution in the brain, lung, and kidney. At the 24 h mark, brain fluorescence measured 7.1 ± 1.8 RFU, liver 23.7 ± 3.1 RFU, spleen 9.5 ± 2.5 RFU, and kidney 4.0 ± 1.7 RFU, with the liver exhibiting the strongest signal and thus serving as the main site of EMV retention at this time point.

Subsequent experiments compared the differential actions of vesicles derived from young versus aged ECs on cerebrovascular aging in both young and old recipient mice. SA-β-gal staining of the basilar artery served as the primary readout for cerebrovascular senescence [34, 35]. Exposure to o.EMVs and o.EEXs led to a substantial rise in senescent cells within the basilar artery wall of y.mice **(Figures 1a and 1g).** In contrast, y.EEXs/y.EMVs in y.mice and o.EEXs/o.EMVs in o.mice elicited no notable changes **(Figures 1a and 1g)**.

Cerebral blood flow (CBF) and blood–brain barrier (BBB) function are recognized indicators of cerebrovascular health [4]. Both y.EMVs and y.EEXs strengthened BBB integrity, while o.EMVs and o.EEXs compromised it, with EMVs producing more robust effects in each direction. No significant alterations occurred with y.EEXs/y.EMVs in y.mice or o.EEXs/o.EMVs in o.mice **(Figures 1b–1d)**. In aged recipients, y.EEXs and y.EMVs elevated CBF, the latter to a greater degree **(Figures 1e and 1h).** As cerebral microvascular density (cMVD) reflects CBF status, CD31-positive endothelial cells were quantified in the hippocampus. Compared with o.mice controls, cMVD increased 3.8 ± 0.03-fold in the y.EMVs group and 2.1 ± 0.02-fold in the y.EEXs group **(Figures 1f and 1i)**. Meanwhile, o.EMVs and o.EEXs diminished CBF in y.mice by 65% and 55%, respectively **(Figures 1e and 1h)**, with o.EMVs inducing a significantly sharper reduction in cMVD than o.EEXs **(Figures 1f and 1i)**. Neither vesicle type from matching age groups affected CBF or cMVD substantially in y.mice or o.mice **(Figures 1e-1f and 1h)**.

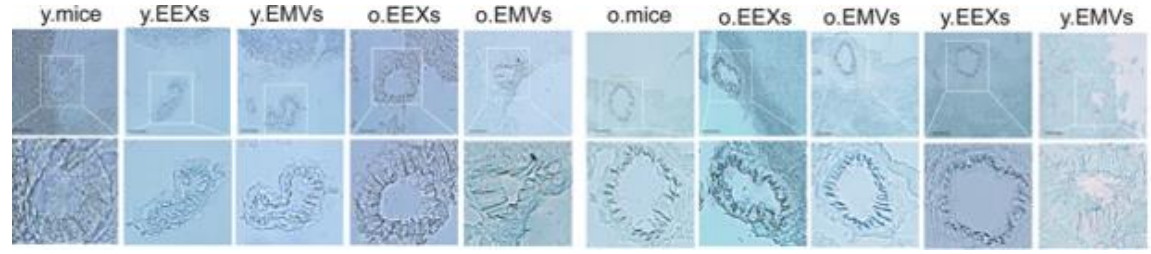

a)

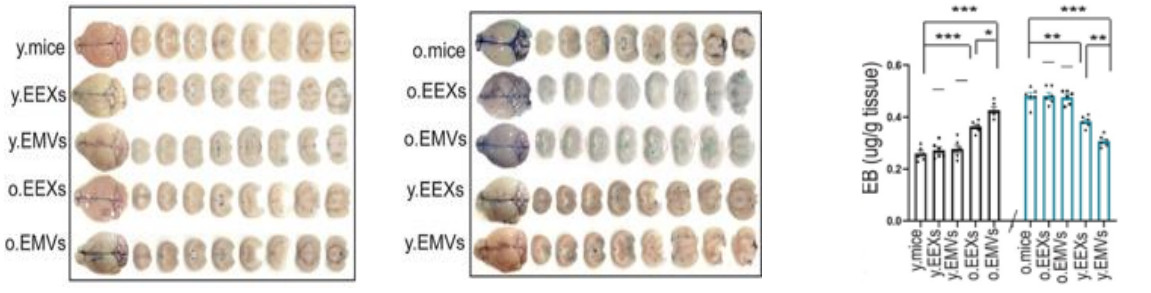

b) c) d)

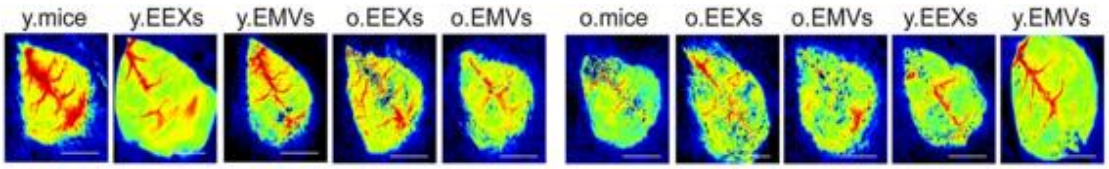

e)

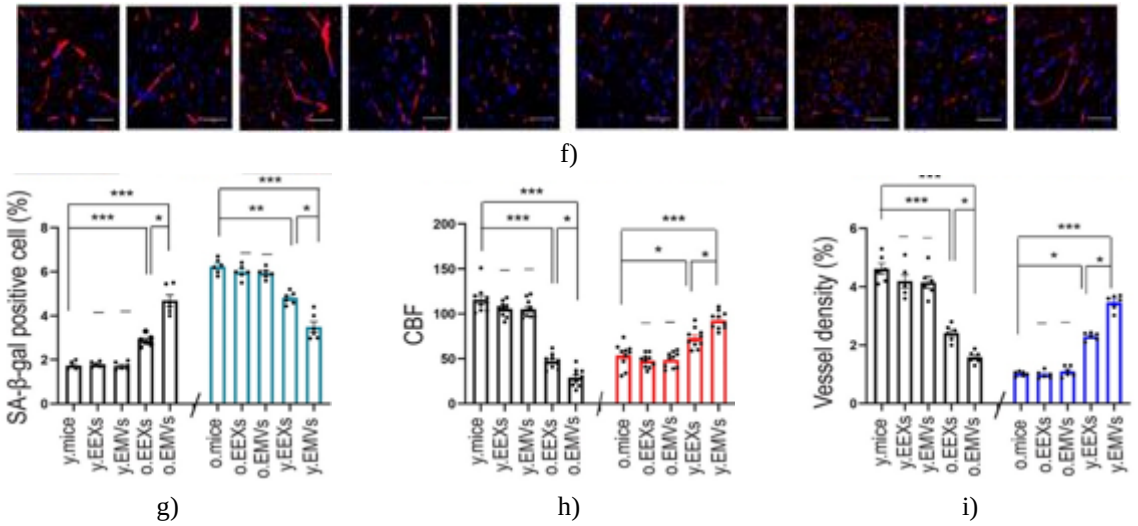

Figure 1. Young-derived EMVs more potently ameliorated cerebrovascular aging, whereas old-derived EMVs more strongly promoted its progression, relative to their EEX counterparts.
(a) Typical photomicrographs of SA-β-gal staining, a hallmark of cellular senescence, in the basilar artery. Blue staining highlighted senescent cells within the vascular smooth muscle and endothelial layers (scale bar = 40 μm, n = 6 biological replicates per group). (b, c) Blood–brain barrier permeability was examined through EB extravasation. (d) EB leakage in mouse brain tissue (one-way ANOVA, Tukey's multiple comparisons test, mean ± SEM, n = 6 biological replicates per group, experiment repeated 3 times; − indicates no significant difference, *p < 0.05, **p < 0.01, ***p < 0.001). (e) Representative laser Doppler flowmetry images of CBF in the various experimental cohorts (scale bar = 0.5 cm, n = 10 biological replicates per group). (f) Confocal micrographs of cerebral microvascular density visualized by CD31+ immunostaining in mouse brains. Red, CD31+; blue, DAPI nuclear stain (scale bar = 50 μm, n = 6 biological replicates per group). (g) Percentage of SA-β-gal-positive cells within the basilar artery (one-way ANOVA, Tukey's multiple comparisons test, mean ± SEM, n = 6 biological replicates per group; − indicates no significant difference, *p < 0.05, ***p < 0.001). (h) Measured CBF values across groups (Kruskal–Wallis ANOVA, post hoc Dunn's multiple comparison test; mean ± SEM, n = 10 biological replicates per group; − indicates no significant difference, *p < 0.05, ***p < 0.001). (i) Vessel density quantification in the studied groups (one-way ANOVA, Tukey's multiple comparisons test, mean ± SEM, n = 6 biological replicates per group; − indicates no significant difference, *p < 0.05, ***p < 0.001). EB, Evans blue; CBF, cerebral blood flow.

Given the established contribution of cerebrovascular decline to broader brain aging [49], the influence of these vesicles on brain senescence was also examined. In y.mice, o.EMVs raised SA-β-gal-positive cell counts in the hippocampal CA3 region by roughly 3.3-fold and o.EEXs by 1.1-fold (**Figures 2a and 2b)**. Both y.EMVs and y.EEXs significantly lowered senescent cell numbers relative to o.mice controls **(Figures 2a and 2b)**. Additional aging indicators—GSSG, MDA, telomerase reverse transcriptase (TERT), and Klotho—were evaluated [50-53]. o.EMVs and o.EEXs elevated plasma GSSG and brain MDA concentrations **(Figures 2c and 2d)** while suppressing Klotho and TERT levels in y.mice brain tissue **(Figures 2e and 2f)**. y.EMVs and y.EEXs produced the inverse pattern across these markers **(Figures 2b–2f),** with EMVs demonstrating stronger modulation of GSSG and Klotho than EEXs.

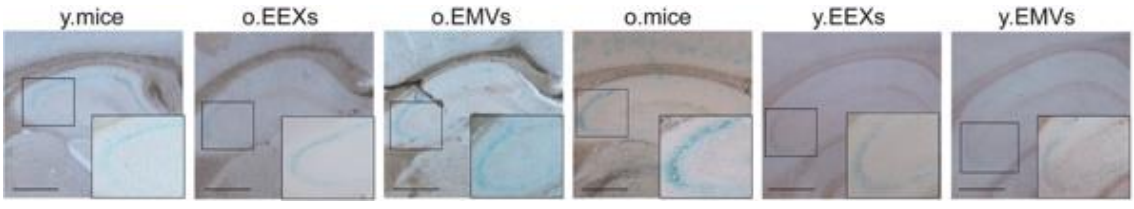

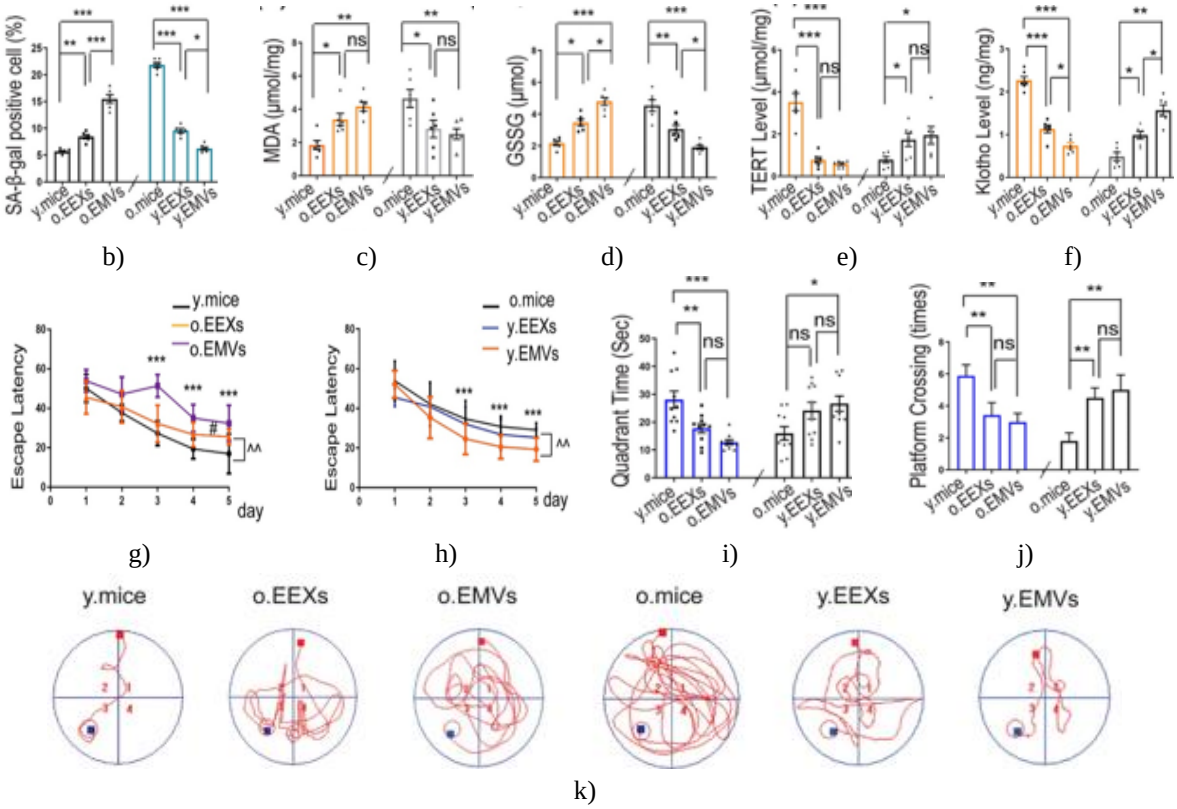

Figure 2. Young EMVs attenuated brain aging, whereas old EMVs accelerated it to a greater extent than young EEXs and old EEXs.

(a) Representative photomicrographs showing SA-β-gal-positive cells within the CA3 hippocampal subfield for each experimental group (scale bar = 100 μm). n = 6 biological replicates per group. (b) Quantitative analysis of SA-β-gal-positive cells among the experimental groups (one-way ANOVA, Tukey's multiple comparisons test, mean ± SEM, n = 6 biological replicates per group, *p < 0.05, **p < 0.01, ***p < 0.001). (c–f) Levels of MDA, telomerase reverse transcriptase, and Klotho expression in the mouse brain (one-way ANOVA, Tukey's multiple comparisons test, mean ± SEM, n = 6 biological replicates per group, *p < 0.05, **p < 0.01, ***p < 0.001, ns, no significance). (g, h) Escape latency across the experimental groups (two-way ANOVA with repeated measures, mean ± SEM, n = 10 biological replicates per group). (i) Time spent in the target quadrant across the experimental groups (one-way ANOVA, Tukey's multiple comparisons test, mean ± SEM, n = 10 biological replicates per group, *p < 0.05, **p < 0.01, ***p < 0.001, ns, no significance). (j) Number of platform crossings among the different groups (Kruskal–Wallis ANOVA, post hoc Dunn's multiple comparison test, mean ± SEM, n = 10 biological replicates per group, **p < 0.01, ns, no significance). (k) Search strategies employed by the different groups (n = 10 biological replicates per group).

Cognitive decline commonly accompanies brain aging [54]. Evaluation via the Morris water maze revealed that o.EMVs and o.EEXs prolonged escape latency, reduced target quadrant occupancy, and disrupted platform crossing and search patterns in y.mice **(Figures 2g, 2i–2k)**. Effects on quadrant time and platform crossings were comparable between o.EMVs and o.EEXs **(Figures 2i and 2j)**. In o.mice, y.EMVs notably shortened escape latency **(Figure 2h)**, extended target quadrant time **(Figure 2i)**, and enhanced platform crossing frequency and search efficiency **(Figures 2j and 2k)**. y.EEXs improved platform crossings **(Figure 2j)** and search strategy **(Figure 2k)** but exerted limited influence on escape latency or quadrant duration **(Figures 2h and 2i)**.

Differential expression of MiR-17-5p in y.EMVs versus o.EMVs

Given that preliminary results demonstrated stronger influences of EMVs on cerebrovascular and brain aging compared to EEXs, the present study directed attention toward the mechanistic actions of EMVs. An initial miRNA sequencing screen was conducted to detect functionally relevant miRNAs contained in EMVs (n = 2/group). The resulting heatmap identified 26 miRNAs that were significantly downregulated and 63 that were upregulated in o.EMVs relative to y.EMVs. MiR-191-3p, miR-196b-5p, and miR-17-5p emerged as the three

most highly enriched miRNAs in y.EMVs when contrasted with o.EMVs. Subsequent qPCR validation assessed the expression of miR-191-3p, miR-196b-5p, and miR-17-5p in both y.EMVs and o.EMVs. Levels of miR-191-3p and miR-196b-5p did not differ significantly between the two EMV types. However, miR-17-5p content within o.EMVs was markedly lower, showing an approximate 52% reduction compared with y.EMVs. Earlier investigations [55] have indicated that miR-17-5p possesses anti-aging properties. Further comparisons confirmed substantially diminished miR-17-5p expression in senescent cells (o.cells) and brain tissues from aged mice (o.mice) in relation to young counterparts (y.cells/y.mice). Administration of y.EMVs produced a pronounced elevation of miR-17-5p in o.cells as well as in the brains of o.mice. By contrast, o.EMVs led to an unexpected decline in miR-17-5p levels within y.cells and the brains of y.mice. Such patterns suggest that the miR-17-5p content in recipient cells is governed by the specific cargo profile of EMVs. To track transfer, a FAM-conjugated peptide nucleic acid (PNA) probe specific for miR-17-5p (FAM-miR-17-5p) was utilized [38]. Experiments revealed that EMVs (red) transporting miR-17-5p (green) were efficiently internalized by cultured cells and by the vascular compartment in the mouse brain. Overall, these observations indicate that EMVs likely operate by transferring miR-17-5p to target tissues.

Y.EMVs suppressed, whereas o.EMVs enhanced cerebrovascular and brain aging via miR-17-5p regulation

To delineate the functional significance of miR-17-5p, targeted genetic silencing (miR-17-5p-KO) was introduced into y.EMVs (y.EMVs$^{miR\text{-}17KO}$), while overexpression was induced in o.EMVs (o.EMVs$^{miR\text{-}17}$) through transduction of y.cells with LV-si-miR-17-5p (y.cells$^{miR\text{-}17KO}$) and o.cells with LV-miR-17-5p (o.cells$^{miR\text{-}17}$) [29]. Post-manipulation assessments confirmed successful miR-17-5p enrichment in o.cells$^{miR\text{-}17}$ and o. o.EMVs$^{miR\text{-}17}$, alongside clear depletion in y.cells$^{miR\text{-}17KO}$ and y.EMVs$^{miR\text{-}17KO}$ relative to scrambled controls.

Subsequent functional tests revealed that o.EMVs$^{miR\text{-}17}$ displayed reduced potency in promoting senescence within basilar artery cells **(Figures 3a and 3g)**, elevating blood–brain barrier permeability **(Figures 3b and 3d)**, and diminishing CBF **(Figures 3e and 3h)** and cMVD **(Figures 3f and 3i)** when compared with unmodified o.EMVs and EMVs$^{miR\text{-}17SC}$. Likewise, y.EMVs$^{miR\text{-}17KO}$ proved less effective than native y.EMVs and EMVs$^{miR\text{-}17KOSC}$ in lowering senescent cell counts in the basilar artery **(Figures 3a and 3g)**, decreasing BBB permeability **(Figures 3c and 3d)**, and augmenting CBF **(Figures 3e and 3h)** and cMVD **(Figures 3f and 3i)**.

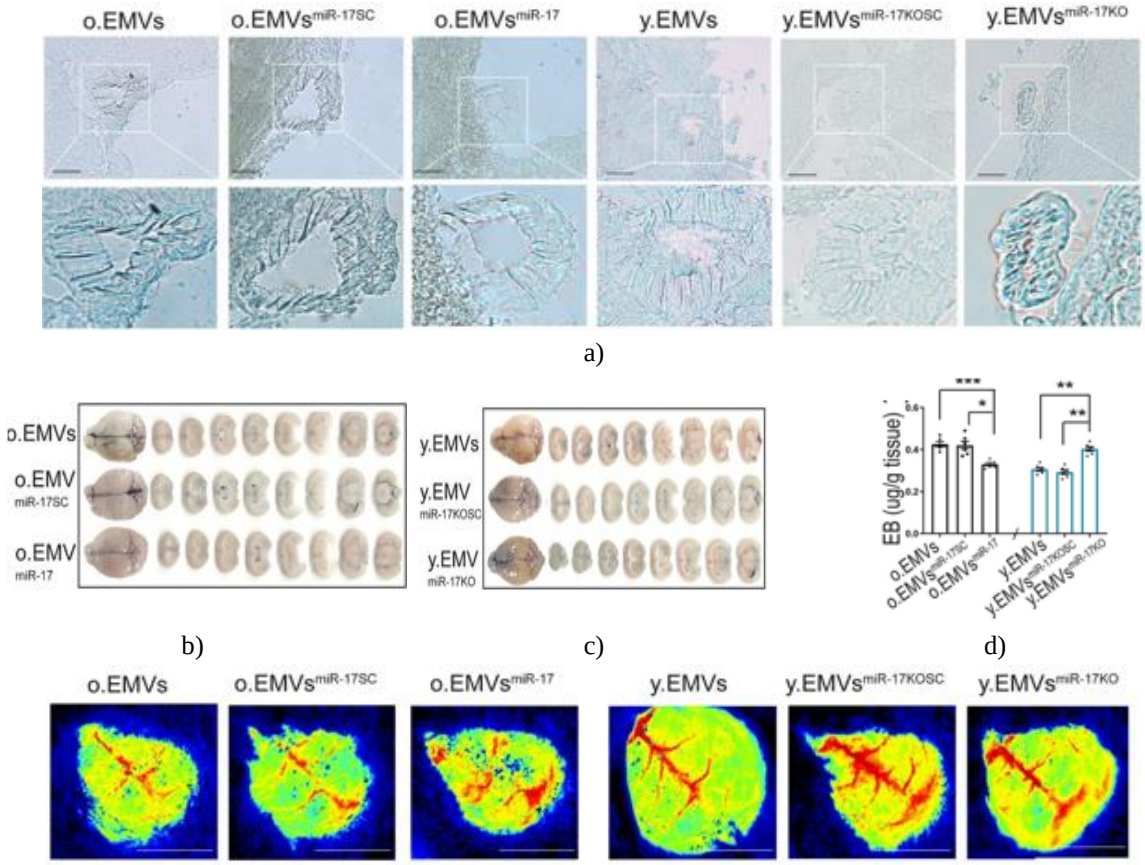

e)

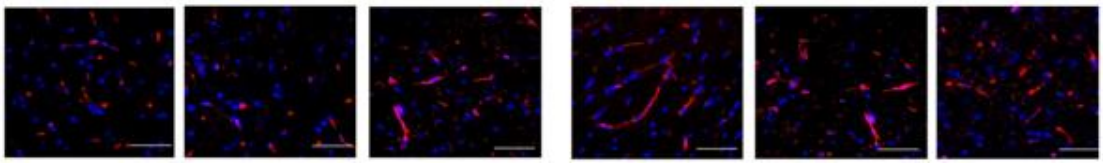

f)

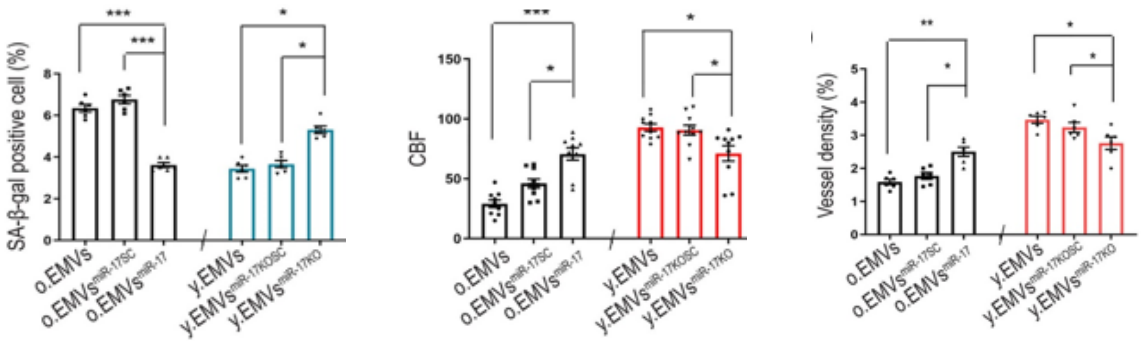

g) h) i)

Figure 3. Y.EMVs mitigated while o.EMVs aggravated cerebrovascular aging through control of miR-17-5p. (a) Representative images of SA-β-gal staining in the basilar artery showing blue-stained cells in the arterial wall smooth muscle or ECs (scale bar = 40 μm, n = 6 biological replicates per group). (b, c) blood brain barrier function was tested using the EB extravasation method. (d) EB extravasation in mouse brains (one-way ANOVA, Tukey's multiple comparisons test, mean ± SEM, n = 6 biological replicates per group, experiment repeated 3 times, *p < 0.05, **p < 0.01, ***p < 0.001). (e) Representative images of CBF measured by laser Doppler flowmetry in different groups (n = 10 biological replicates per group). (f) Confocal microscopy images of cMVD indicated by CD31+ cells in mouse brains. Red, CD31+; blue, DAPI for nuclear staining (scale bar = 50 μm, n = 6 biological replicates per group). (g) The percentage of SA-β-gal-positive cells in the basilar artery (one-way ANOVA, Tukey's multiple comparisons test, mean ± SEM, n = 6 biological replicates per group, *p < 0.05, ***p < 0.001). (h) Quantification of CBF in various groups (Kruskal–Wallis ANOVA, post hoc Dunn's multiple comparison test, mean ± SEM, n = 10 biological replicates per group, *p < 0.05, ***p < 0.001). (i) Quantification of vessel density in various groups (one-way ANOVA, Tukey's multiple comparisons test, mean ± SEM, n = 6 biological replicates per group, *p < 0.05, **p < 0.01). EB, Evans blue; CBF, cerebral blood flow.

These cerebrovascular outcomes were mirrored in brain aging parameters. Compared with o.EMVs and o.EMVs^{miR-17}, o.EMVs$^{miR-17SC}$ showed attenuated effects on raising hippocampal senescent cell numbers **(Figures 4a and 4b)**, increasing plasma GSSG and brain MDA levels, and suppressing Klotho and TERT expression in the brain **(Figures 4c–4f)**. In addition, o.EMVs^{miR-17} were less capable of extending escape latency **(Figure 4g)**, reducing target quadrant occupancy and platform crossings, and impairing search strategy **(Figures 4i–4k)**. In parallel, o.EMVs$^{miR-17SC}$ exerted weaker protective actions than y.EMVs and y.EMVs$^{miR-17KO}$ by showing limited efficacy in reducing senescent cells, MDA, and GSSG while elevating TERT and Klotho **(Figures 4a–4f)**. They were also less effective at decreasing escape latency, boosting platform crossings and target quadrant time, and optimizing search strategy **(Figures 4h–4k)**. In conclusion, EMVs appear to regulate cerebrovascular and brain aging primarily by modulating miR-17-5p levels.

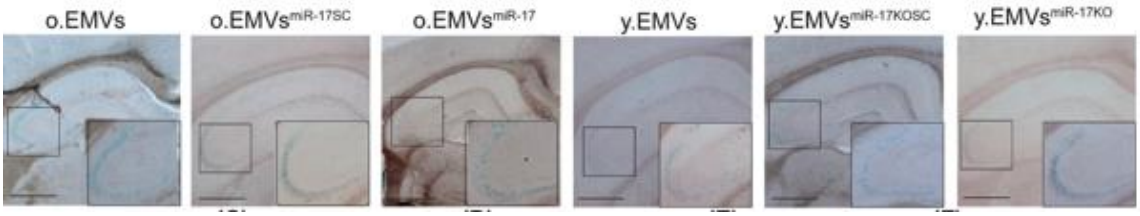

a)

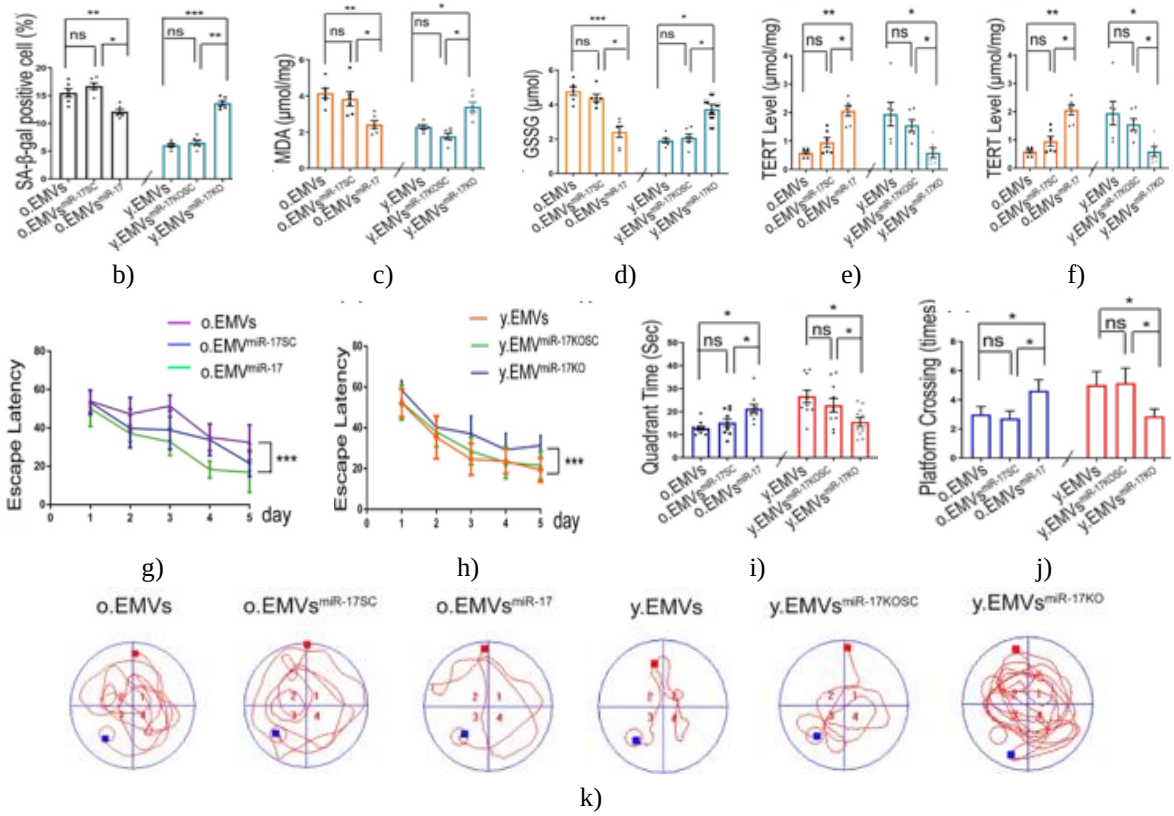

Figure 4. Y.EMVs ameliorated while o.EMVs intensified brain aging by modulating miR-17-5p. (a) Representative images of SA-β-gal-positive cells in the CA3 region of the hippocampus in different groups. Blue staining shows the presence of senescent cells (scale bar = 100 μm). n = 6 biological replicates per group. (b) Quantification of SA-β-gal-positive cells in various groups (one-way ANOVA, Tukey's multiple comparisons test, mean ± SEM, n = 6 biological replicates per group, *p < 0.05, **p < 0.01, ***p < 0.001). (c–f) Mouse brain MDA, telomerase reverse transcriptase and Klotho expression and plasma levels of GSSG (one-way ANOVA, Tukey's multiple comparisons test, mean ± SEM, n = 6 biological replicates per group, *p < 0.05, **p < 0.01, ***p < 0.001, ns, no significance). (g, h) Escape latency of various groups (two-way ANOVA with repeated measures, mean ± SEM, n = 10 biological replicates per group). (i) Time spent in the target quadrant of various groups (one-way ANOVA, Tukey's multiple comparisons test, mean ± SEM, n = 10 biological replicates per group, *p < 0.05, ns, no significance). (j) The number of platform crossings of different groups (Kruskal–Wallis ANOVA, post hoc Dunn's multiple comparison test, mean ± SEM, n = 10 biological replicates per group, *p < 0.05, ns, no significance). (k) Search strategy for different groups (n = 10 biological replicates per group).

Furthermore, an adeno-associated virus serotype 9 (AAV9) vector carrying miR-17-5p under the control of the endothelium-specific TIE promoter (TIEmiR-17-5p AAV9) was generated to examine the contribution of endothelial miR-17-5p to vascular and brain aging [56]. Overexpression of miR-17-5p specifically in the endothelium of aged mice substantially reduced senescence in both the basilar artery and hippocampus **(Figures 5a and 5d, and 5d-5e)**. It also restored CBF **(Figures 5c and 5f)**, improved cognitive performance **(Figures 6b–6e)**, and normalized brain aging indicators, including GSSG, MDA, TERT, and Klotho levels **(Figures 5g–5j)**. Conversely, endothelial-specific knockdown of miR-17-5p in young mice markedly promoted senescence in the basilar artery and hippocampus, impaired CBF and cognitive function, and worsened brain aging markers **(Figures 5 and 6)**.

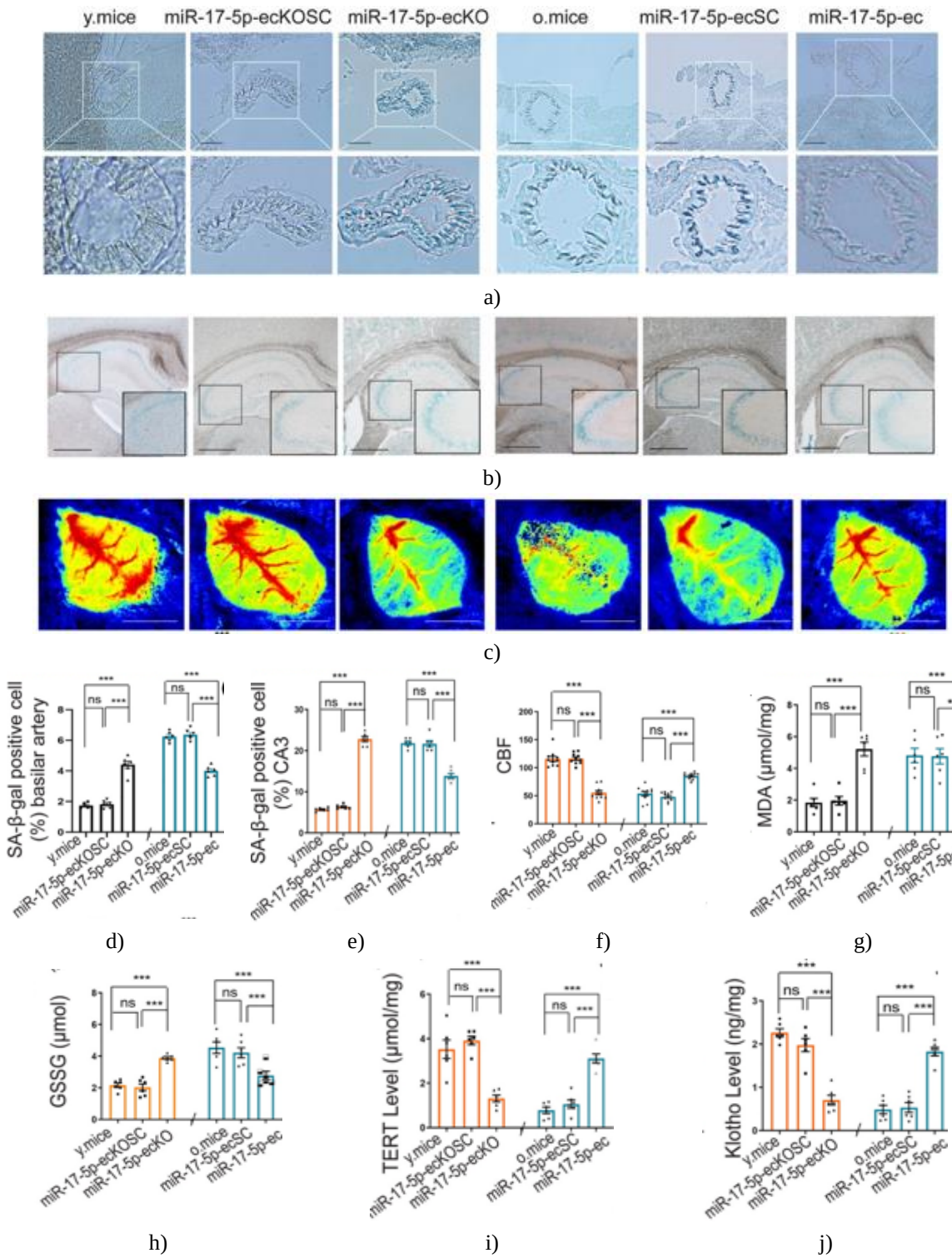

Figure 5. Endothelium-targeted overexpression of miR-17-5p alleviated, whereas endothelium-targeted deletion of miR-17-5p aggravated cerebrovascular and brain aging. (a, b) Representative images of SA-β-gal staining in the basilar artery and CA3 region of the hippocampus (scale bar = 40 μm for the basilar artery; scale bar = 100 μm for CA3; n = 6 biological replicates per group). (c) Representative images of CBF measured by laser Doppler flowmetry in different groups (n = 10 biological replicates per group). (d, e) Summary data of SA-β-gal staining in the basilar artery and CA3 region of the hippocampus (one-way ANOVA, Tukey's multiple comparisons test, mean ± SEM, n = 6 biological replicates per group, ***p < 0.001, ns, no significance). (f) Quantification of CBF in various groups (one-way ANOVA, Tukey's multiple comparisons test, mean ± SEM, n = 10 biological replicates per group, ***p < 0.001, ns, no significance). (g–j) Mouse plasma GSSG levels and brain MDA, telomerase reverse transcriptase, and Klotho expression

across groups (one-way ANOVA, Tukey's multiple comparisons test, mean ± SEM, n = 6 biological replicates per group, **p < 0.01, ***p < 0.001, ns, no significance). CBF, cerebral blood flow.

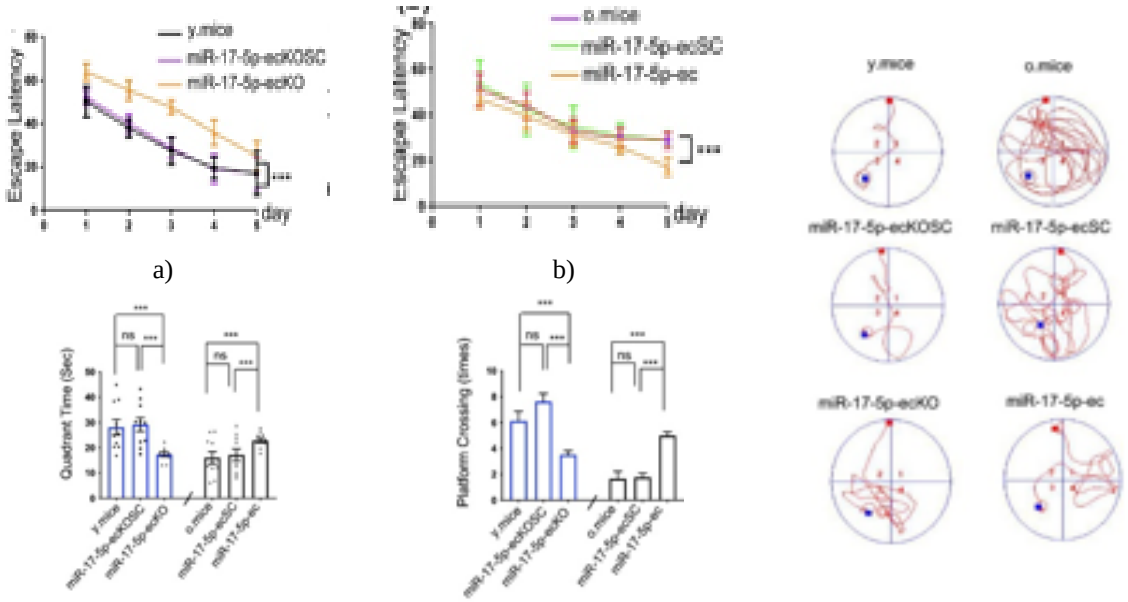

Figure 6. Endothelium-specific overexpression of miR-17-5p improved, while endothelium-specific knockdown of miR-17-5p impaired cognitive performance.

(a, b) Escape latency of various groups (two-way ANOVA with repeated measures, mean ± SEM, n = 10 biological replicates per group). (c) Time spent in the target quadrant of various groups (one-way ANOVA, Tukey's multiple comparisons test, mean ± SEM, n = 10 biological replicates per group, ***p < 0.001, ns, no significance). (d) The number of platform crossings of different groups (Kruskal–Wallis ANOVA, post hoc Dunn's multiple comparison test, mean ± SEM, n = 10 biological replicates per group, ***p < 0.001, ns, no significance). (e) Searching strategy for different groups (n = 10 biological replicates per group).

Y.EMVs reduced, while o.EMVs intensified oxidative stress and apoptosis in the mouse brain vasculature through miR-17-5p modulation

Oxidative stress and apoptotic pathways play central roles in aging [8]. To explore the mechanisms underlying EMV actions, reactive oxygen species (ROS), nitric oxide (NO), and TUNEL staining were performed on mouse hippocampal sections (including both overview and high-magnification views) **(Figures 7a–7o)**. Administration of o.EMVs markedly elevated ROS **(Figures 7a and 7g and 7i)** and apoptotic signals **(Figures 7c and 7j and 7l)** while suppressing NO production in the vasculature of hippocampal slices from young mice **(Figures 7e and 7m and 7o)**. In contrast, y.EMVs substantially lowered ROS **(Figures 7b and 7h and 7i)** and apoptosis levels **(Figures 7d and 7k and 7l)** and enhanced NO generation in the vasculature of hippocampal slices from aged mice **(Figures 7f and 7n and 7o)**. Manipulating miR-17-5p levels through overexpression or knockdown substantially attenuated the effects of o.EMVs or y.EMVs, respectively, as well as those of their corresponding scrambled controls **(Figures 7a–7o)**.

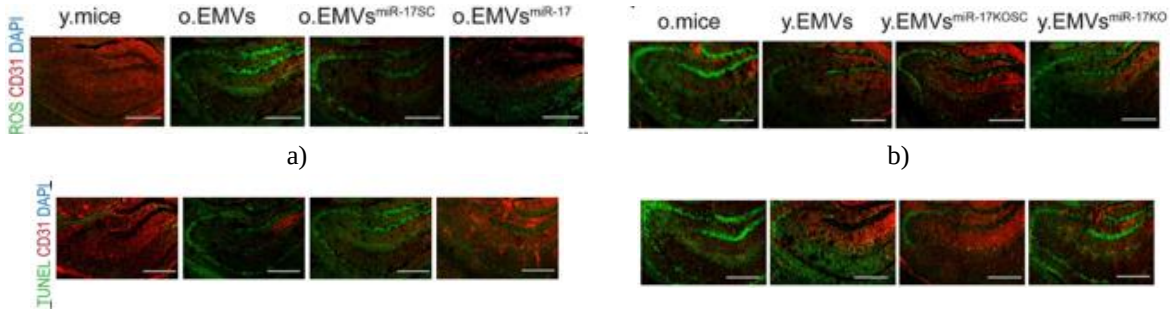

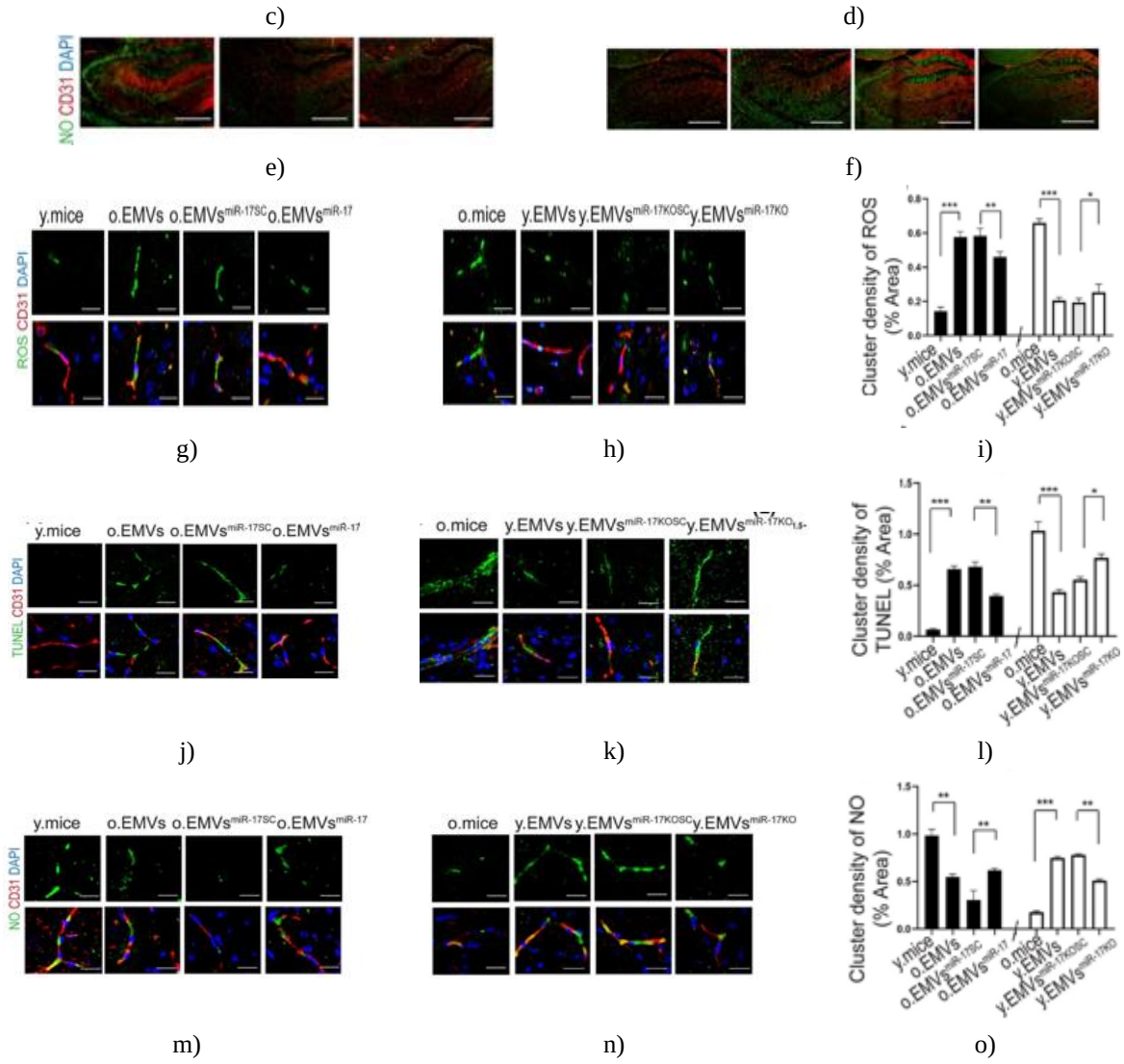

Figure 7. Y.EMVs attenuated, while o.EMVs promoted oxidative stress and apoptosis in the mouse brain vasculature by modulating miR-17-5p.

(a, b) Representative low-magnification images of ROS staining in mouse hippocampal blood vessels (red: CD31, green: ROS; scale bar = 120 μm. n = 6 biological replicates per group). (c, d) Representative low-magnification images of TUNEL-stained mouse hippocampal blood vessels (red: CD31+, green: TUNEL; scale bar = 120 μm. n = 6 biological replicates per group). (e, f) Representative low-magnification images of NO staining in mouse hippocampal blood vessels (red: CD31+, green: NO; scale bar = 120 μm. n = 6 biological replicates per group). (g, h) Representative images of costaining for CD31+ (red) and ROS (green) across groups. CD31 served as an endothelial marker, with DAPI (blue) used for nuclear counterstaining (scale bar = 30 μm. n = 6 biological replicates per group). (i) Summary of ROS levels in mouse brain vasculature (one-way ANOVA, Tukey's multiple comparisons test, mean ± SEM, n = 6 biological replicates per group, *p < 0.05, **p < 0.01, ***p < 0.001). (j, k) Immunofluorescence costaining of CD31+ (red) and TUNEL (green) in mouse brain vasculature across groups. TUNEL served as a marker of apoptosis (scale bar = 30 μm. n = 6 biological replicates per group). (l) Summary of apoptotic levels in mouse brain vasculature (one-way ANOVA, Tukey's multiple comparisons test, mean ± SEM, n = 6 biological replicates per group, *p < 0.05, **p < 0.01, ***p < 0.001). (m, n) Immunofluorescence costaining of CD31 (red) with NO (green) across groups (scale bar = 30 μm. n = 6 biological replicates per group). (o) Summary of NO levels in mouse brain vasculature (one-way ANOVA, Tukey's multiple comparisons test, mean ± SEM, n = 6 biological replicates per group, **p < 0.01, ***p < 0.001). NO, nitric oxide; ROS, reactive oxygen species.

Y.EMVs safeguarded, whereas o.EMVs aggravated BMEC senescence and dysfunction through modulation of the miR-17-5p/PI3K/Akt signaling axis

Immunofluorescence analysis demonstrated efficient uptake of PKH26-labeled EMVs and EEXs (red) by BMECs following 8 h of co-incubation. Subsequent functional assays were conducted to determine whether EMVs influence BMEC senescence and physiological performance. Key senescence-associated markers include P16, P21, and P53, with telomere attrition representing a central mechanism in this process [57]. Exposure to o.EMVs strongly induced senescence, as indicated by heightened SA-β-gal activity, upregulated expression of P16, P21, and P53 proteins, and shortened telomere length **(Figures 8a and 8c-8g)**. Additionally, o.EMVs elevated ROS and apoptotic rates **(Figures 8h and 8j and 8k)** while suppressing NO production **(Figures 8h and 8l)**, along with impairing proliferation **(Figure 9d)**, migration **(Figures 9a and 9c)**, and tube-forming capacity in y.cells **(Figures 9e and 9g)**. Relative to native o.EMVs and o.EMVs$^{miR\text{-}17SC}$, the o.EMVs$^{miR\text{-}17}$ variant exerted milder detrimental impacts on y.cells **(Figures 8 and 9)**. In contrast, y.EMVs effectively lowered senescent cell populations and reduced P16, P21, and P53 protein abundance while extending telomere length **(Figures 8b–8g)**. These vesicles also suppressed ROS generation and apoptosis **(Figures 8h–8k)**, enhanced NO levels **(Figures 8i and 8l)**, and stimulated proliferation **(Figure 9d)**, migration **(Figures 9b and 9c)**, and tube formation in o.cells **(Figures 9f and 9g)**. The Y.EMVs$^{miR\text{-}17KO}$ displayed reduced protective efficacy compared with native y.EMVs and y.EMVs$^{miR\text{-}17KOSC}$ **(Figures 8 and 9)**.

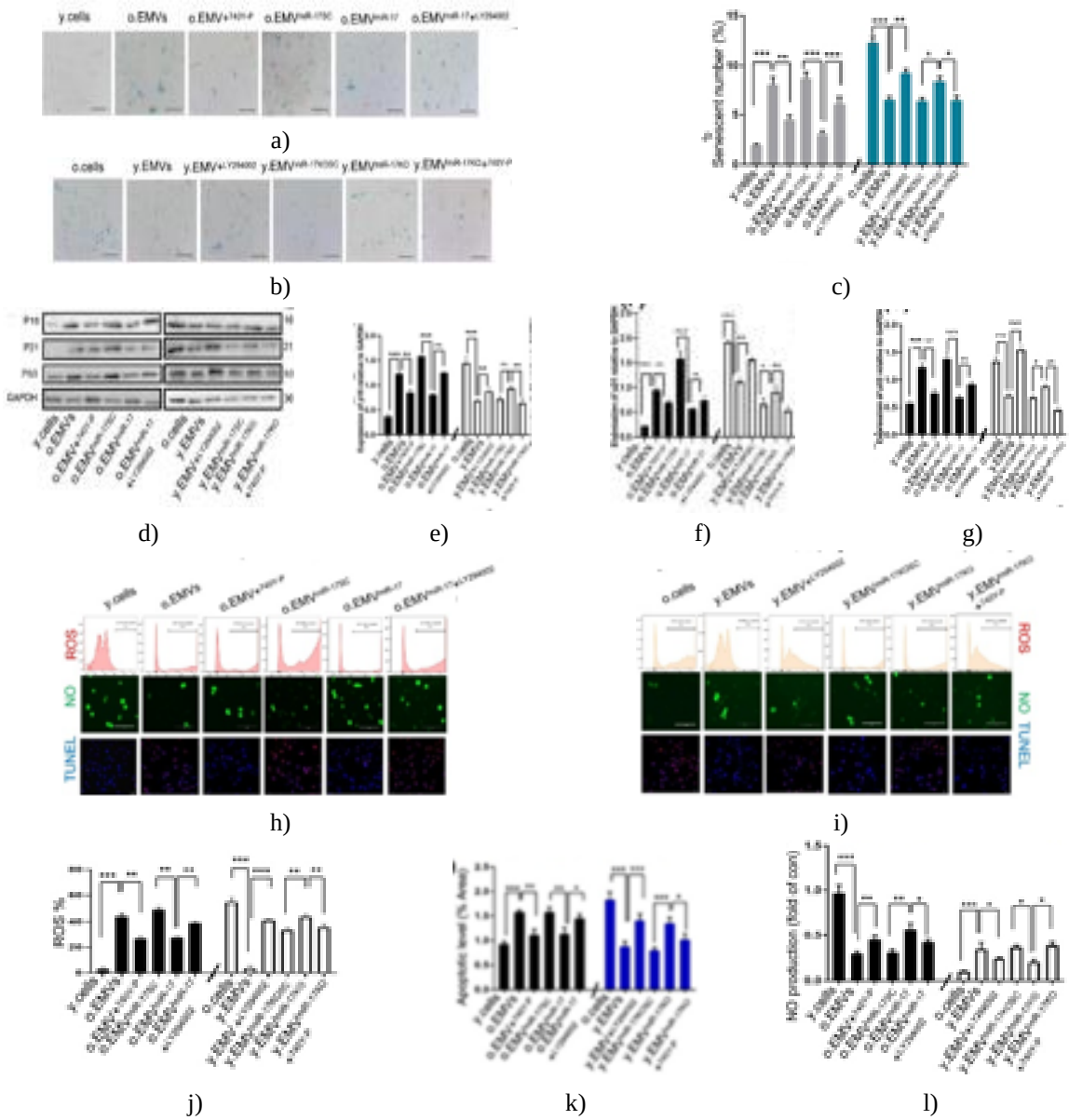

Figure 8. Y.EMVs and o.EMVs regulated brain microvascular endothelial cell senescence, oxidative stress, and apoptosis via the miR-17-5p/PI3K/Akt pathway.
(a, b) Representative images of SA-β-gal staining in diverse groups (scale bar = 200 μm). (c) Quantification of SA-β-gal-positive cells in various groups (one-way ANOVA, Tukey's multiple comparisons test, mean ± SEM, n = 3 technical replicates, *p < 0.05, **p < 0.01, ***p < 0.001). (d) Western blotting images of senescent proteins P16, P21 and P53. (e–g) Quantification of P16, P21 and P53 in various groups. (h, i) Representative images of ROS, NO and apoptosis in the y.cells and o.cells in the various groups, as assessed by FACS, DAF-FM DA and TUNEL staining (scale bar = 200 μm for NO, scale bar = 20 μm for TUNEL. The red and blue staining in TUNEL indicates apoptotic cells and nucleus). (j-l) Summary of ROS, apoptosis and NO expression in various groups (one-way ANOVA, Tukey's multiple comparisons test, mean ± SEM, n = 3 technical replicates, *p < 0.05, **p < 0.01, ***p < 0.001). NO, nitric oxide; ROS, reactive oxygen species.

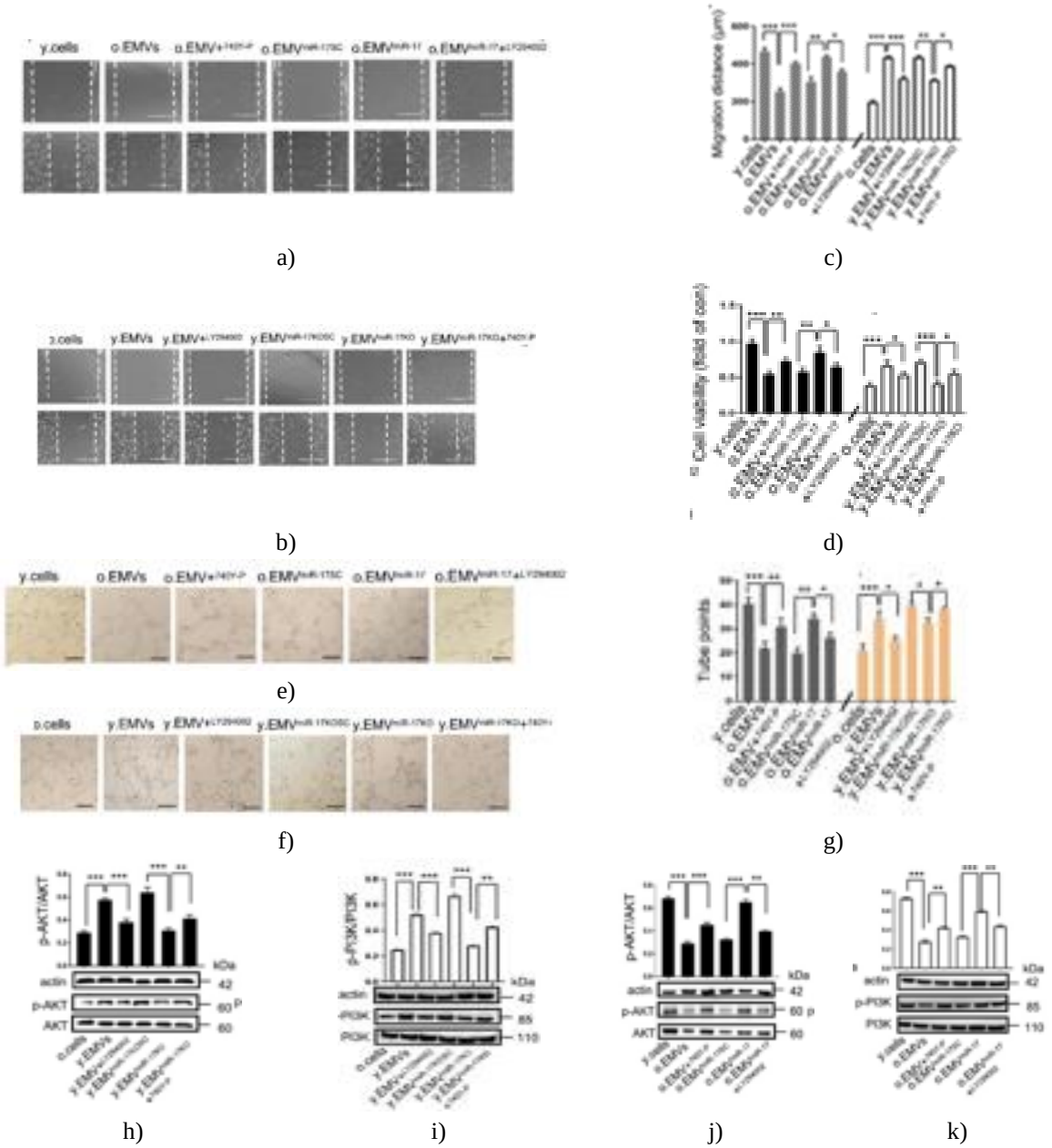

Figure 9. Y.EMVs improved, while o.EMVs impaired BMEC migration, proliferation and tube formation by controlling the miR-17-5p/PI3K/Akt pathway.
(a, b) Representative images of the scratch assay showing BMEC migration (scale bar, 400 μm). (c) Quantification of BMEC migration (one-way ANOVA, Tukey's multiple comparisons test, mean ± SEM, n =

3 technical replicates, *p < 0.05, **p < 0.01, ***p < 0.001). (d) CCK-8 assay of BMEC proliferation (one-way ANOVA, Tukey's multiple comparisons test, mean ± SEM, n = 3 technical replicates, *p < 0.05, **p < 0.01, ***p < 0.001). (e, f) Representative images of BMEC tube formation (scale bar, 200 μm). (g) Summarized data of tube points per field (one-way ANOVA, Tukey's multiple comparisons test, mean ± SEM, n = 3 technical replicates, *p < 0.05, **p < 0.01, ***p < 0.001). (h–k) Western blotting was used to analyze the protein levels of p-PI3K/PI3K and p-Akt/Akt in various groups (one-way ANOVA, Tukey's multiple comparisons test, mean ± SEM, n = 3 technical replicates, **p < 0.01, ***p < 0.001). BMEC, brain microvascular endothelial cell.

From a mechanistic perspective, ingenuity pathway analysis (IPA) identified strong associations between miR-17-5p activity and the PI3K/Akt signaling cascade. Gene ontology (GO) enrichment further linked miR-17-5p to processes such as protein kinase A signaling, synaptic plasticity, neurite extension, and cellular migration. Bioinformatics prediction using available databases (http://mirwalk.umm.uni-heidelberg.de/) nominated PI3K as a direct target of miR-17-5p, a relationship subsequently validated through Dual-Luciferase Reporter Assay. Western blot analyses showed that o.EMVs substantially lowered p-PI3K/PI3K and p-Akt/Akt ratios in y.cells **(Figures 9j and 9k)**. In comparison with o.EMVs and o.EMVs$^{miR\text{-}17SC}$, o.EMVs$^{miR\text{-}17}$ increased these phosphorylation ratios **(Figures 9j and 9k)**. Meanwhile, y.EMVs robustly enhanced p-PI3K/PI3K and p-Akt/Akt levels in o.cells **(Figures 9h and 9i)**, whereas Y.EMVs$^{miR\text{-}17KO}$ produced the opposite effect relative to y.EMVs and controls **(Figures 9h and 9i)**.

To validate the involvement of the PI3K/Akt axis, pharmacological modulation was performed using the PI3K inhibitor LY-294002 and the activator 740Y-P. Treatment with 740Y-P effectively counteracted the detrimental actions of o.EMVs on BMEC senescence **(Figures 8a–8g)** as well as on ROS, NO, apoptosis, migration, proliferation, and tube formation **(Figures 8h–8l and 9a–9g)**, concurrent with restored p-Akt/Akt and p-PI3K/PI3K signaling **(Figures 9j and 9k)**. Conversely, LY-294002 largely abolished the beneficial influences of y.EMVs on senescence **(Figures 8b–8g)** and endothelial functions **(Figures 8h–8l and 9a–9g)**, accompanied by reduced pathway activation **(Figures 9h and 9i)**. Notably, LY-294002-treated o.EMVs$^{miR\text{-}17}$ displayed stronger senescence-promoting and functional-impairing effects than untreated o.EMVs$^{miR\text{-}17}$ but remained less potent than native o.EMVs **(Figures 8h–8l and 9a–9g)**. Similarly, 740Y-P supplementation enhanced the anti-senescence and functional-protective capacity of y.EMVs$^{miR\text{-}17KO}$ beyond that of the unmodified knockdown vesicles, yet not to the full extent observed with native y.EMVs **(Figures 8h–8l and 9a–9g)**. Collectively, these findings indicate that EMVs govern BMEC senescence, oxidative injury, apoptosis, and angiogenic deficits primarily by modulating the miR-17-5p/PI3K/Akt signaling pathway.

Clinical subject characteristics

Following the identification of differential expression patterns for EMVs and EMV-miR-17-5p in cultured cells and mouse models, the translational relevance of these vesicles and their cargo was examined in human plasma specimens. The study recruited 119 individuals, comprising 50 females and 69 males. These participants were stratified into three age categories: young adults (18–45 years, n = 58), middle-aged adults (46–65 years, n = 33), and older adults (>65 years, n = 28). Notable intergroup differences emerged with respect to chronological age, carotid intima-media thickness (IMT), circulating EMV abundance, and EMV-encapsulated miR-17-5p content.

Plasma EMV, EMV-miR-17-5p, and ROS concentrations exhibited age-dependent patterns, independent of sex

Particle size analysis indicated that plasma EMVs (defined as CD105+CD144+ microvesicles) displayed comparable dimensions across the young, middle-aged, and aged cohorts. Quantitative assessment revealed that EMV concentrations in aged individuals were roughly 2.5 times higher than in young subjects and 1.6 times higher than in middle-aged subjects, whereas levels between the young and middle-aged groups did not differ significantly **(Figure 10a)**. These observations mirrored results obtained from in vitro cell models and murine experiments. Levels of miR-17-5p within circulating EMVs were markedly lower in the aged group compared with young participants, though they did not differ from the middle-aged cohort **(Figure 10b)**. Plasma ROS concentrations were also elevated in aged individuals relative to both younger groups, with the greatest increase observed in the oldest participants **(Figure 10c)**. Correlation studies demonstrated that ROS levels positively associated with EMV concentrations **(Figure 10d)**, ($r = 0.51$, $p < 0.001$) and inversely associated with EMV-miR-17-5p levels **(Figure 10e)**, ($r = -0.45$, $p < 0.001$). Additional analyses stratified by sex confirmed the absence of

significant differences in EMV counts between males and females, with equivalent levels observed in both sexes among individuals younger than 45 years and those older than 45 years.

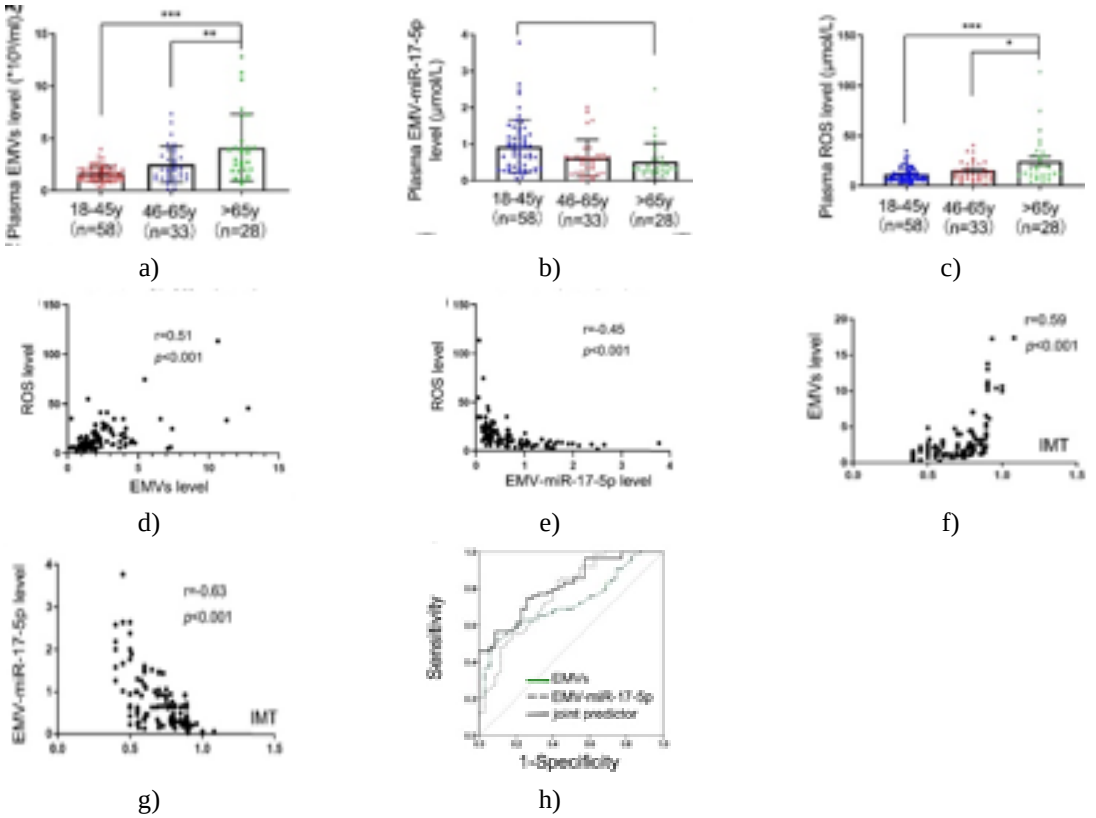

Figure 10. Plasma EMV and EMV-miR-17-5p concentrations changed with advancing age and showed associations with vascular aging indicators and ROS; both parameters possessed considerable diagnostic potential for detecting vascular aging.

(a) Plasma levels of EMVs in different groups tested by NTA (18–45 years old, n = 58; 46–65 years old, n = 33; >65 years old, n = 28) (Kruskal–Wallis ANOVA, post hoc Dunn's multiple comparison test, mean ± SEM, **p < 0.01, ***p < 0.001). (b) Plasma levels of EMV-miR-17-5p in various groups were assessed by qPCR (Kruskal–Wallis ANOVA, post hoc Dunn's multiple comparison test; mean ± SEM, **p < 0.01). (c) Plasma levels of ROS in different groups (Kruskal–Wallis ANOVA, post hoc Dunn's multiple comparison test, mean ± SEM, *p < 0.05, ***p < 0.001). (d, e) Correlation analysis of the levels of EMVs and EMV-miR-17-5p with ROS. (f, g) Correlation analysis of the levels of EMVs (n = 119) and EMV-miR-17-5p (n = 119) with IMT. Correlations between variables were determined by Spearman correlation analysis. (h) ROC analysis was used to assess the diagnostic value of EMVs, EMV-miR-17-5p and their combination for vascular aging defined by IMT. IMT, intima-media thickness; ROS, reactive oxygen species.

Plasma EMV and EMV-miR-17-5p levels correlated with IMT and exhibited strong diagnostic utility for vascular aging

Carotid intima-media thickness (IMT) represents a well-established surrogate measure of vascular aging [1, 44]. Spearman rank correlation analysis uncovered a moderate positive link between circulating EMV levels and IMT **(Figure 10f)**, ($r = 0.59$, $p < 0.001$), while EMV-miR-17-5p content displayed a robust negative correlation with this parameter **(Figure 10g)**, ($r = -0.63$, $p < 0.001$).

Receiver operating characteristic (ROC) curve analysis, presented in **Figure 10h**, evaluated the capacity of EMVs and EMV-miR-17-5p to discriminate vascular aging, defined according to an IMT threshold of >0.58 mm [1, 44-46]. Individual AUC values were 0.724 for EMVs (sensitivity 51.8%, specificity 91.4%) and 0.77 for EMV-miR-17-5p (sensitivity 84.3%, specificity 57.1%). When combined, the two markers achieved an AUC of 0.815 (sensitivity 74.7%, specificity 74.3%). These data collectively support the potential application of plasma EMVs and EMV-miR-17-5p as accessible biomarkers for the assessment of vascular aging.

This investigation revealed that y.EMVs effectively counteracted cerebrovascular aging. This was demonstrated through the suppression of vascular senescence, the prevention of CBF decline, and the maintenance of BBB integrity. The vesicles also mitigated brain aging by lowering the abundance of senescent cells in the hippocampus, modulating key aging indicators (TERT, Klotho, MDA, and GSSG), and improving cognitive performance in mice. By comparison, o.EMVs produced the reverse outcomes. Notably, EMVs elicited more robust responses than EEXs. Mechanistic analyses indicated that y.EMVs hindered cerebrovascular aging, whereas o.EMVs accelerated it, primarily by altering miR-17-5p abundance. In addition, y.EMVs diminished endothelial cell senescence and bolstered endothelial cell viability, resistance to oxidative stress, and survival by stimulating the miR-17-5p/PI3K/Akt signaling cascade, with o.EMVs displaying antagonistic actions.

From a clinical perspective, circulating EMV concentrations rose substantially in healthy subjects beyond 65 years of age and displayed a positive association with the vascular aging parameter IMT. In contrast, EMV-associated miR-17-5p levels declined in older adults and correlated negatively with IMT. Plasma ROS concentrations showed a positive relationship with EMV levels and an inverse relationship with EMV-miR-17-5p content. In summary, young endothelial cells release EMVs that impede vascular aging by relieving endothelial senescence and functional impairment through activation of the miR-17-5p/PI3K/Akt pathway, which in turn restrains brain aging. Senescent endothelial cells, however, generate EMVs with detrimental properties, marked by higher vesicle release and diminished miR-17-5p packaging. Both EMVs and their miR-17-5p cargo hold considerable promise as biomarkers of vascular aging. These results offer valuable insights into potential strategies for detecting and intervening in cerebrovascular and brain aging processes.

Vascular aging underlies numerous vascular disorders that place considerable strain on healthcare resources [3, 4]. The identification of dependable clinical biomarkers for vascular senescence continues to represent a critical gap in medical practice. EMVs and EEXs have gained recognition as key participants and potential diagnostic tools in vascular conditions including stroke, diabetes, and kidney disease [58, 59]. Nevertheless, their specific connection to vascular aging has remained unclear. The present work provides initial evidence that y.EMVs and y.EEXs markedly lowered the number of senescent cells in the basilar artery, while o.EMVs and o.EEXs raised it, with EMVs showing a stronger impact. These observations point to an important regulatory function of EMVs and EEXs in cerebrovascular aging.

Progression of cerebrovascular aging compromises CBF and BBB function [4, 60]. Earlier reports documented reductions of roughly 15% in cerebral microvessel density and 33% in CBF among aged mice [61]. Dynamic contrast-enhanced MRI further confirmed heightened BBB permeability within the hippocampus of elderly individuals [62]. Here, administration of y.EMVs and y.EEXs enhanced cerebrovascular density, restored CBF, and strengthened BBB integrity in old mice, whereas o.EMVs and o.EEXs induced adverse changes in young animals. These results imply that EMVs and EEXs secreted by young endothelial cells exert rejuvenating effects on the cerebrovasculature, but those originating from aged endothelial cells promote progressive deterioration. The superior potency of EMVs over EEXs observed in this study merits additional mechanistic inquiry.

Recent studies have highlighted differences in the transcriptomic content of exosomes versus microvesicles isolated from human umbilical cord mesenchymal stem cells [63], which may underlie the divergent contributions of EMVs and EEXs during aging due to variations in their molecular payloads. The current findings are consistent with prior reports demonstrating that EMVs derived from senescent porcine heart endothelial cells triggered endothelial senescence [64], and that EEXs from aged human umbilical vein endothelial cells promoted senescence in vascular smooth muscle cells [65]. Utilizing primary cerebral endothelial cells, this study uniquely establishes that EMVs exert more potent control over cerebrovascular aging than EEXs.

Cerebrovascular aging exerts a major influence on the development of brain aging [4, 60]. The effects of EMVs and EEXs on brain aging were therefore also assessed. SA-β-gal staining indicated that y.EMVs and y.EEXs reduced hippocampal cellular senescence, while o.EMVs and o.EEXs elevated it. Neurovascular decline associated with aging involves structural damage and functional loss that ultimately impair cognition [60]. In Morris water maze assessments, y.EMVs and y.EEXs improved cognitive performance, whereas o.EMVs and o.EEXs worsened it. EMVs produced clearer benefits than EEXs on parameters of spatial memory such as escape latency and search strategy, but both vesicle populations yielded similar results for measures of long-term memory including target quadrant occupancy and platform crossings. This pattern suggests differential modulation of spatial learning capacity alongside comparable influences on long-term memory retention [66].

Evaluation of hippocampal aging-related molecules demonstrated that y.EMVs and y.EEXs decreased senescent cell counts, lowered MDA and GSSG concentrations, and raised TERT and Klotho expression in aged mice, with

o.EMVs and o.EEXs eliciting opposing shifts. EMVs outperformed EEXs in the regulation of GSSG and Klotho. MDA and GSSG function as oxidative stress indicators strongly associated with aging and have been found at higher levels in the hippocampus of aged rodents [31, 32]. Klotho is widely regarded as an anti-aging gene that supports antioxidant defense and curbs inflammation; its enhanced expression extends murine lifespan [33]. TERT helps preserve telomere integrity, thereby limiting oxidative injury and cellular senescence [52, 53]. No meaningful distinctions emerged between EMVs and EEXs concerning MDA and TERT modulation, indicating potentially shared actions on lipid peroxidation and telomerase function [53, 67].

Taken together, y.EMVs proved superior to EEXs in attenuating brain aging, while o.EMVs displayed stronger aggravating potential. This distinction likely relates to differential control of oxidative stress pathways. Supporting evidence comes from parabiosis experiments, which showed that exposure to young circulatory factors restored neurogenesis and cognition in old mice [68], suggesting that blood-borne elements such as y.EMVs may serve as primary mediators of rejuvenation.

Emerging evidence has identified miRNAs as important mediators of the biological effects of EMVs [9, 11, 12]. Our miRNA sequencing data indicated that miR-17-5p abundance was markedly reduced in o.EMVs relative to y.EMVs. As a prominent member of the miR-17-92 cluster, miR-17-5p functions as a conserved modulator of cellular senescence [55, 69]. This miRNA is enriched in embryonic stem cell-derived EVs, where it helps rescue age-related deficits in neurogenesis [70]. Transgenic overexpression of miR-17 prolongs lifespan in mice and diminishes the accumulation of senescent cells in various tissues, including skin, lung, kidney, and heart [55]. Reduced miR-17-5p expression represents a characteristic feature of stress-induced premature senescence in human diploid fibroblasts and human trabecular meshwork cells [71]. Moreover, elevated miR-17 levels inhibit apoptosis and enhance tube formation in HUVECs [72]. The present results support a protective role for miR-17-5p against vascular endothelial dysfunction and aging.

In this study, endothelium-specific knockdown and overexpression experiments in young and old mice confirmed the essential contribution of miR-17-5p to endothelial cell-mediated regulation of brain aging. We observed significantly higher miR-17-5p levels in young brain endothelial cells, brain tissue, and y.EMVs compared with their aged counterparts. Treatment with y.EMVs elevated miR-17-5p concentrations in mouse brain tissue and senescent endothelial cells. These observations establish that miR-17-5p is preferentially expressed in young brain endothelial cells, packaged into EMVs, and transferred to target endothelial cells, while its expression declines in senescent endothelial cells from old mice. Notably, o.EMVs may deliver additional negative regulators of miR-17-5p beyond simply reducing its quantity; the precise mechanisms responsible for the pro-aging actions of o.EMVs require further clarification. Functional experiments demonstrated that forced expression of miR-17-5p in o.EMVs or depletion of miR-17-5p in y.EMVs substantially attenuated the adverse or beneficial impacts on cerebrovascular and brain aging, respectively. These findings underscore the central role of miR-17-5p in mediating the effects of EMVs.

Endothelial cell senescence and dysfunction constitute early hallmarks of cerebrovascular and brain aging [1]. We therefore examined the influence and mechanisms of EMVs on endothelial cells. Results showed that y.EMVs significantly reduced, while o.EMVs increased, endothelial cell senescence; these changes were partially reversed by modulating miR-17-5p levels through downregulation or overexpression. Collectively, these data indicate that EMVs exert differential control over endothelial cell senescence during aging via regulation of miR-17-5p. Oxidative stress and apoptosis represent central processes driving vascular aging and endothelial cell senescence [8]. Excessive oxidative stress disrupts endothelial homeostasis, impairs BBB integrity, promotes cerebral edema, and compromises cerebral perfusion [7, 73]. Furthermore, elevated endothelial cell apoptosis contributes to reduced CBF, BBB disruption, and vascular aging [4, 29]. Key mediators of oxidative stress include endothelial cell apoptosis, ROS production, and NO generation. Quantitative analyses revealed that y.EMVs attenuated oxidative damage and apoptosis, whereas o.EMVs exacerbated these processes in cultured endothelial cells and brain slice preparations. This pattern is consistent with the known ability of heightened oxidative stress to promote apoptosis [73]. Such bidirectional modulation mirrors EV-mediated regulation of the aging microenvironment, whereby y.EMVs suppress and o.EMVs amplify pro-senescence signals in recipient cells.

In addition, endothelial cell migration, proliferation, and tube formation are essential for angiogenesis and vascular network expansion [5]. Diminished angiogenic capacity and vessel density correlate with reduced CBF [4]. In the present study, y.EMVs enhanced the angiogenic potential of endothelial cells, while o.EMVs suppressed it. Upregulation of miR-17-5p in o.EMVs or its downregulation in y.EMVs markedly diminished these

respective effects on endothelial cell functions. Overall, these findings demonstrate that EMVs regulate endothelial cell senescence and function through miR-17-5p, thereby influencing vascular and brain aging.

Pathway analysis using IPA identified strong associations between miR-17-5p activity and members of the PI3K family as well as Akt. The PI3K/Akt pathway constitutes a classical signaling cascade with multifaceted regulatory roles. Previous work from our group has established its involvement in ROS/NO generation, apoptosis, cell migration, and proliferation [29, 74]. The current results showed that y.EMVs increased, while o.EMVs decreased, p-PI3K/PI3K and p-Akt/Akt ratios in senescent and young endothelial cells, respectively; these alterations were dependent on miR-17-5p levels. Pharmacological inhibition or activation of PI3K significantly blocked the downstream effects of o.EMVs or y.EMVs combined with miR-17-5p modulation on p-Akt/Akt levels, endothelial cell senescence, and function. Treatment with the PI3K inhibitor LY-294002 or activator 740Y-P attenuated but did not fully abolish the actions of y.EMVs/o.EMVs and o.EMVmiR-17/y.EMVmiR-17KO on endothelial cell behavior, suggesting that the PI3K/Akt pathway plays a major but not exclusive role in mediating the effects of EMVs and miR-17-5p. On the basis of these observations, y.EMVs and o.EMVs appear to counteract or promote cerebrovascular and brain aging, respectively, through activation or suppression of the miR-17-5p/PI3K/Akt signaling axis.

This comprehensive analysis revealed a pronounced elevation of EMVs in the culture medium of high-passage endothelial cells and in the plasma of aged mice exhibiting vascular aging. Compared with y.EMVs and young endothelial cells, miR-17-5p content was substantially lower in o.EMVs and senescent endothelial cells. These observations suggest that EMV quantity and EMV-miR-17-5p levels may serve as potential biomarkers for vascular aging. Consistent with the preclinical data, clinical samples from aged individuals showed significantly increased EMV levels and decreased EMV-miR-17-5p levels. These changes correlated positively and negatively with chronological age, respectively. Plasma ROS concentrations were also elevated in older subjects and displayed positive or negative associations with EMV and EMV-miR-17-5p levels, linking these vesicles to oxidative stress. It is important to note that chronological aging does not invariably parallel vascular aging. Clinically, carotid intima-media thickness (IMT) serves as an established indicator of vascular aging, with values exceeding 0.58 mm signifying vascular aging in healthy populations [1, 44-46]. One limitation of the present study is that IMT measurements can be influenced by operator experience. Additional vascular aging indicators should be investigated. Blood-based biomarkers offer advantages in terms of objectivity and reproducibility [75], and venous blood sampling is routine in clinical settings. Correlation analyses in this study confirmed that plasma EMV levels were positively associated with IMT, while EMV-miR-17-5p levels were negatively associated. Receiver operating characteristic (ROC) curve analysis supported the diagnostic utility of both EMVs and EMV-miR-17-5p for vascular aging, with EMV-miR-17-5p showing superior performance and the combined biomarker yielding the highest accuracy. These clinical findings align with the in vivo and in vitro results, reinforcing the concept that EMVs from young endothelial cells exert rejuvenating effects on vascular and brain aging, whereas those from senescent cells operate through alternative mechanisms. EMVs and EMV-miR-17-5p therefore represent promising biomarkers for vascular aging.

Biodistribution studies indicated that EMVs accumulated predominantly in the brain within the first 4 h post-administration and shifted primarily to the liver thereafter. This temporal pattern suggests that the observed effects on brain vasculature result from both direct and indirect actions of EMVs. Future research exploring liver-brain axis communication via EVs would be valuable [76]. It is also recognized that the in vivo distribution of EVs can be modulated by temporal and environmental factors [77]. Consequently, more refined methodologies are needed for the accurate characterization and quantification of EVs in vitro and in vivo. In subsequent investigations, techniques such as nanopore sequencing and nanoscale liquid chromatography coupled to tandem mass spectrometry (Nano LC–MS/MS) could be employed to comprehensively profile the RNA and protein cargo of EMVs and EEXs. Additionally, mitochondrial dysfunction is a critical driver of senescence, warranting dedicated studies in future work. Finally, validation in larger cohorts encompassing diverse ethnic backgrounds and geographic latitudes will be necessary to strengthen these conclusions.

Conclusion

In summary, the present study demonstrated that EMVs exert more potent regulatory effects on vascular aging than EEXs. EMVs released by young endothelial cells attenuate vascular and brain aging by alleviating endothelial cell senescence and preserving endothelial cell functions through the miR-17-5p/PI3K/Akt pathway. In contrast,

EMVs derived from senescent endothelial cells produce opposing effects. Plasma EMVs and their encapsulated miR-17-5p represent promising biomarkers for vascular aging. These findings provide novel mechanistic insights and potential therapeutic avenues for the management of vascular and brain aging.

Acknowledgments: None

Conflict of Interest: None

Financial Support: None

Ethics Statement: None

References

1. Hamczyk MR, Nevado RM, Barettino A, Fuster V, Andrés V. Biological versus chronological aging: JACC focus seminar. J Am Coll Cardiol. 2020;75(8):919-30. doi:10.1016/j.jacc.2019.11.062
2. Van Skike CE, Lin AL, Roberts Burbank R, Halloran JJ, Hernandez SF, Cuvillier J, et al. mTOR drives cerebrovascular, synaptic, and cognitive dysfunction in normative aging. Aging Cell. 2020;19(1):e13057. doi:10.1111/acel.13057
3. Katan M, Luft A. Global burden of stroke. Semin Neurol. 2018;38(2):208-11. doi:10.1055/s-0038-1649503
4. Yang T, Sun Y, Lu Z, Leak RK, Zhang F. The impact of cerebrovascular aging on vascular cognitive impairment and dementia. Ageing Res Rev. 2017;34:15-29. doi:10.1016/j.arr.2016.09.007
5. Rossman MJ, Kaplon RE, Hill SD, McNamara MN, Santos-Parker JR, Pierce GL, et al. Endothelial cell senescence with aging in healthy humans: Prevention by habitual exercise and relation to vascular endothelial function. Am J Physiol Heart Circ Physiol. 2017;313(5):H890-5. doi:10.1152/ajpheart.00416.2017
6. Liberale L, Montecucco F, Tardif JC, Libby P, Camici GG. Inflamm-ageing: The role of inflammation in age-dependent cardiovascular disease. Eur Heart J. 2020;41(31):2974-82. doi:10.1093/eurheartj/ehz961
7. An L, Shen Y, Chopp M, Zacharek A, Venkat P, Chen Z, et al. Deficiency of endothelial nitric oxide synthase (eNOS) exacerbates brain damage and cognitive deficit in a mouse model of vascular dementia. Aging Dis. 2021;12(3):732-46. doi:10.14336/AD.2020.0523
8. Wang Y, Wang JM, Xiao Y, Hu XB, Zheng SY, Fu JL, et al. SUMO1-regulated DBC1 promotes p53-dependent stress-induced apoptosis of lens epithelial cells. Aging (Albany NY). 2023;15(17):8812-32. doi:10.18632/aging.205001
9. Yin Y, Chen H, Wang Y, Zhang L, Wang X. Roles of extracellular vesicles in the aging microenvironment and age-related diseases. J Extracell Vesicles. 2021;10(12):e12154. doi:10.1002/jev2.12154
10. Frühbeis C, Kuo-Elsner WP, Müller C, Barth K, Peris L, Tenzer S, et al. Oligodendrocytes support axonal transport and maintenance via exosome secretion. PLoS Biol. 2020;18(12):e3000621. doi:10.1371/journal.pbio.3000621
11. Zietzer A, Hosen MR, Wang H, Goody PR, Sylvester M, Latz E, et al. The RNA-binding protein hnRNPU regulates the sorting of microRNA-30c-5p into large extracellular vesicles. J Extracell Vesicles. 2020;9(1):1786967. doi:10.1080/20013078.2020.1786967
12. Bei Y, Das S, Rodosthenous RS, Holvoet P, Vanhaverbeke M, Monteiro MC, et al. Extracellular vesicles in cardiovascular theranostics. Theranostics. 2017;7(17):4168-77. doi:10.7150/thno.21274
13. Ma X, Wang J, Li J, Ma C, Chen S, Lei W, et al. Loading miR-210 in endothelial progenitor cells derived exosomes boosts their beneficial effects on hypoxia/reoxygenation-injured human endothelial cells via protecting mitochondrial function. Cell Physiol Biochem. 2018;46(2):664-75. doi:10.1159/000488635
14. Pan Q, Ma C, Wang Y, Wang J, Zheng J, Du D, et al. Microvesicles-mediated communication between endothelial cells modulates endothelial survival and angiogenic function via transferring of miR-125a-5p. J Cell Biochem. 2019;120(3):3160-72. doi:10.1002/jcb.27581
15. Bammert TD, Hijmans JG, Reiakvam WR, Levy MV, Brewster LM, Goldthwaite ZA, et al. High glucose derived endothelial microparticles increase active caspase-3 and reduce microRNA-Let-7a expression in endothelial cells. Biochem Biophys Res Commun. 2017;493(2):1026-9. doi:10.1016/j.bbrc.2017.09.098

16. Chung J, Kim KH, Yu N, An SH, Lee S, Kwon K. Fluid shear stress regulates the landscape of microRNAs in endothelial cell-derived small extracellular vesicles and modulates the function of endothelial cells. Int J Mol Sci. 2022;23(3):1314. doi:10.3390/ijms23031314
17. Gröne M, Sansone R, Höffken P, Horn P, Rodriguez-Mateos A, Schroeter H, et al. Cocoa flavanols improve endothelial functional integrity in healthy young and elderly subjects. J Agric Food Chem. 2020;68(7):1871-6. doi:10.1021/acs.jafc.9b02251
18. Villeda SA, Plambeck KE, Middeldorp J, Castellano JM, Mosher KI, Luo J, et al. Young blood reverses age-related impairments in cognitive function and synaptic plasticity in mice. Nat Med. 2014;20(6):659-63. doi:10.1038/nm.3569
19. Jansen F, Yang X, Hoelscher M, Cattelan A, Schmitz T, Proebsting S, et al. Endothelial microparticle-mediated transfer of microRNA-126 promotes vascular endothelial cell repair via SPRED1 and is abrogated in glucose-damaged endothelial microparticles. Circulation. 2013;128(18):2026-38. doi:10.1161/CIRCULATIONAHA.113.001720
20. Gollmann-Tepeköylü C, Pölzl L, Graber M, Hirsch J, Nägele F, Lobenwein D, et al. miR-19a-3p containing exosomes improve function of ischaemic myocardium upon shock wave therapy. Cardiovasc Res. 2020;116(6):1226-36. doi:10.1093/cvr/cvz209
21. Bittner S, Ruck T, Schuhmann MK, Herrmann AM, Moha ou Maati H, Bobak N, et al. Endothelial TWIK-related potassium channel-1 (TREK1) regulates immune-cell trafficking into the CNS. Nat Med. 2013;19(9):1161-5. doi:10.1038/nm.3303
22. Dubinsky AN, Dastidar SG, Hsu CL, Zahra R, Djakovic SN, Duarte S, et al. Let-7 coordinately suppresses components of the amino acid sensing pathway to repress mTORC1 and induce autophagy. Cell Metab. 2014;20(4):626-38. doi:10.1016/j.cmet.2014.09.001
23. Sakamuri SSVP, Sure VN, Kolli L, Liu N, Evans WR, Sperling JA, et al. Glycolytic and oxidative phosphorylation defects precede the development of senescence in primary human brain microvascular endothelial cells. GeroScience. 2022;44(4):1975-94. doi:10.1007/s11357-022-00550-2
24. Zhang H, Chen G, Qiu W, Pan Q, Chen Y, Chen Y, et al. Plasma endothelial microvesicles and their carrying miRNA-155 serve as biomarkers for ischemic stroke. J Neurosci Res. 2020;98(11):2290-301. doi:10.1002/jnr.24696
25. Pan Q, Kuang X, Cai S, Wang X, Du D, Wang J, et al. miR-132-3p priming enhances the effects of mesenchymal stromal cell-derived exosomes on ameliorating brain ischemic injury. Stem Cell Res Ther. 2020;11(1):260. doi:10.1186/s13287-020-01761-0
26. Lázaro-Ibáñez E, Neuvonen M, Takatalo M, Thanigai Arasu U, Capasso C, Cerullo V, et al. Metastatic state of parent cells influences the uptake and functionality of prostate cancer cell-derived extracellular vesicles. J Extracell Vesicles. 2017;6(1):1354645. doi:10.1080/20013078.2017.1354645
27. Yang C, Chen F, Ren P, Lofchy L, Wan C, Shen J, et al. Delivery of a model lipophilic membrane cargo to bone marrow via cell-derived microparticles. J Control Release. 2020;326:324-34. doi:10.1016/j.jconrel.2020.07.019
28. Vorhees CV, Williams MT. Morris water maze: procedures for assessing spatial and related forms of learning and memory. Nat Protoc. 2006;1(2):848-58. doi:10.1038/nprot.2006.116
29. Zhang H, Pan Q, Xie Z, Chen Y, Wang J, Bihl J, et al. Implication of MicroRNA503 in brain endothelial cell function and ischemic stroke. Transl Stroke Res. 2020;11(5):1148-64. doi:10.1007/s12975-020-00794-0
30. Yamazaki Y, Baker DJ, Tachibana M, Liu CC, van Deursen JM, Brott TG, et al. Vascular cell senescence contributes to blood-brain barrier breakdown. Stroke. 2016;47(4):1068-77. doi:10.1161/STROKEAHA.115.010835
31. Almeida EB, Santos JMB, Paixão V, Amaral JB, Foster R, Sperandio A, et al. L-Glutamine supplementation improves the benefits of combined-exercise training on oral redox balance and inflammatory status in elderly individuals. Oxid Med Cell Longev. 2020;2020:2852181. doi:10.1155/2020/2852181
32. Szlęzak D, Bronowicka-Adamska P, Hutsch T, Ufnal M, Wróbel M. Hypertension and aging affect liver sulfur metabolism in rats. Cells. 2021;10(5):1238. doi:10.3390/cells10051238
33. Kurosu H, Yamamoto M, Clark JD, Pastor JV, Nandi A, Gurnani P, et al. Suppression of aging in mice by the hormone Klotho. Science. 2005;309(5742):1829-33. doi:10.1126/science.1112766

34. Stoodley M, Weihl CC, Zhang ZD, Lin G, Johns LM, Kowalczuk A, et al. Effect of adenovirus-mediated nitric oxide synthase gene transfer on vasospasm after experimental subarachnoid hemorrhage. Neurosurgery. 2000;46(5):1193-202. doi:10.1097/00006123-200005000-00034
35. Onoue H, Tsutsui M, Smith L, Stelter A, O'Brien T, Katusic ZS. Expression and function of recombinant endothelial nitric oxide synthase gene in canine basilar artery after experimental subarachnoid hemorrhage. Stroke. 1998;29(9):1959-65. doi:10.1161/01.str.29.9.1959
36. Wang F, Lu J, Peng X, Wang J, Liu X, Chen X, et al. Integrated analysis of microRNA regulatory network in nasopharyngeal carcinoma with deep sequencing. J Exp Clin Cancer Res. 2016;35:17. doi:10.1186/s13046-016-0292-4
37. Baciu C, Sage A, Zamel R, Shin J, Bai XH, Hough O, et al. Transcriptomic investigation reveals donor-specific gene signatures in human lung transplants. Eur Respir J. 2021;57(4):2000327. doi:10.1183/13993003.00327-2020
38. Song Y, Zhang C, Zhang J, Jiao Z, Dong N, Wang G, et al. Localized injection of miRNA-21-enriched extracellular vesicles effectively restores cardiac function after myocardial infarction. Theranostics. 2019;9(8):2346-60. doi:10.7150/thno.29945
39. Chang J, Yao Y, Sun X, Wang W, Qian H, Liu Y, et al. JAG1 mediates apoptosis in herpes simplex keratitis by suppressing autophagy via ROS/JAG1/NOTCH1/pULK1 signaling pathway. Cell Biol Toxicol. 2024;41(1):1. doi:10.1007/s10565-024-09968-0
40. Zhao B, Yu J, Luo Y, Xie M, Qu C, Shi Q, et al. Deficiency of S100 calcium binding protein A9 attenuates vascular dysfunction in aged mice. Redox Biol. 2023;63:102721. doi:10.1016/j.redox.2023.102721
41. Radavelli-Bagatini S, Blekkenhorst LC, Sim M, Prince RL, Bondonno NP, Bondonno CP, et al. Fruit and vegetable intake is inversely associated with perceived stress across the adult lifespan. Clin Nutr. 2021;40(5):2860-7. doi:10.1016/j.clnu.2021.03.043
42. Rubega M, Formaggio E, Di Marco R, Bertuccelli M, Tortora S, Menegatti E, et al. Cortical correlates in upright dynamic and static balance in the elderly. Sci Rep. 2021;11(1):14132. doi:10.1038/s41598-021-93556-3
43. Fedintsev A, Kashtanova D, Tkacheva O, Strazhesko I, Kudryavtseva A, Baranova A, et al. Markers of arterial health could serve as accurate non-invasive predictors of human biological and chronological age. Aging (Albany NY). 2017;9(4):1280-92. doi:10.18632/aging.101227
44. van Sloten TT, Boutouyrie P, Lisan Q, Tafflet M, Thomas F, Guibout C, et al. Body silhouette trajectories across the lifespan and vascular aging. Hypertension. 2018;72(5):1095-102. doi:10.1161/HYPERTENSIONAHA.118.11442
45. Andreassi MG, Piccaluga E, Gargani L, Sabatino L, Borghini A, Faita F, et al. Subclinical carotid atherosclerosis and early vascular aging from long-term low-dose ionizing radiation exposure: a genetic, telomere, and vascular ultrasound study in cardiac catheterization laboratory staff. JACC Cardiovasc Interv. 2015;8(4):616-27. doi:10.1016/j.jcin.2014.12.233
46. Engelen L, Ferreira I, Stehouwer CD, Boutouyrie P, Laurent S. Reference intervals for common carotid intima-media thickness measured with echotracking: relation with risk factors. Eur Heart J. 2013;34(30):2368-80. doi:10.1093/eurheartj/ehs380
47. Xu B, Fu Y, Liu Y, Agvanian S, Wirka RC, Baum R, et al. The ESCRT-III pathway facilitates cardiomyocyte release of cBIN1-containing microparticles. PLoS Biol. 2017;15(8):e2002354. doi:10.1371/journal.pbio.2002354
48. Lenna S, Bellotti C, Duchi S, Martella E, Columbaro M, Dozza B, et al. Mesenchymal stromal cells mediated delivery of photoactive nanoparticles inhibits osteosarcoma growth in vitro and in a murine in vivo ectopic model. J Exp Clin Cancer Res. 2020;39(1):40. doi:10.1186/s13046-020-01548-4
49. Greenberg SM. Vascular contributions to brain health: cross-cutting themes. Stroke. 2022;53(2):391-3. doi:10.1161/STROKEAHA.121.034921
50. Naguib M, Feldman N, Zarodkiewicz P, Shropshire H, Biamis C, El-Halfawy OM, et al. An evolutionary conserved detoxification system for membrane lipid-derived peroxyl radicals in Gram-negative bacteria. PLoS Biol. 2022;20:e3001610. doi:10.1371/journal.pbio.3001610
51. Sharma M, Pandey R, Saluja D. ROS is the major player in regulating altered autophagy and lifespan in sin-3 mutants of C. elegans. Autophagy. 2018;14(7):1239-55. doi:10.1080/15548627.2018.1474312

52. Baeeri M, Didari T, Khalid M, Mohammadi-Nejad S, Daghighi SM, Farhadi R, et al. Molecular evidence of the inhibitory potential of melatonin against NaAsO2-induced aging in male rats. Molecules. 2021;26(21):6603. doi:10.3390/molecules26216603
53. Li J, Liu HT, Zhao J, Chen HJ. Telomerase reverse transcriptase (TERT) promotes neurogenesis after hypoxic-ischemic brain damage in neonatal rats. Neurol Res. 2022;44(9):819-29. doi:10.1080/01616412.2022.2056339
54. Stakos DA, Stamatelopoulos K, Bampatsias D, Sachse M, Zormpas E, Vlachogiannis NI, et al. The Alzheimer's disease amyloid-beta hypothesis in cardiovascular aging and disease: JACC focus seminar. J Am Coll Cardiol. 2020;75(8):952-67. doi:10.1016/j.jacc.2019.12.033
55. Du WW, Yang W, Fang L, Xuan J, Li H, Khorshidi A, et al. miR-17 extends mouse lifespan by inhibiting senescence signaling mediated by MKP7. Cell Death Dis. 2014;5(7):e1355. doi:10.1038/cddis.2014.305
56. Bei Y, Lu D, Bär C, Chatterjee S, Costa A, Riedel I, et al. miR-486 attenuates cardiac ischemia/reperfusion injury and mediates the beneficial effect of exercise for myocardial protection. Mol Ther. 2022;30(4):1675-91. doi:10.1016/j.ymthe.2022.01.031
57. Zhang H, Xiao X, Wang L, Shi X, Fu N, Wang S, et al. Human adipose and umbilical cord mesenchymal stem cell-derived extracellular vesicles mitigate photoaging via TIMP1/Notch1. Signal Transduct Target Ther. 2024;9:294. doi:10.1038/s41392-024-01990-0
58. Otero-Ortega L, Laso-García F, Gómez-de Frutos M, Fuentes B, Diekhorst L, Díez-Tejedor E, et al. Role of exosomes as a treatment and potential biomarker for stroke. Transl Stroke Res. 2019;10(3):241-9. doi:10.1007/s12975-018-0654-7
59. Rodrigues KF, Pietrani NT, Fernandes AP, Bosco AA, de Sousa MCR, Oliveira Silva IF, et al. Circulating microparticles levels are increased in patients with diabetic kidney disease: a case-control research. Clin Chim Acta. 2018;479:48-55. doi:10.1016/j.cca.2017.12.048
60. Cortes-Canteli M, Iadecola C. Alzheimer's disease and vascular aging: JACC focus seminar. J Am Coll Cardiol. 2020;75(8):942-51. doi:10.1016/j.jacc.2019.10.062
61. Li Y, Choi WJ, Wei W, Song S, Zhang Q, Liu J, et al. Aging-associated changes in cerebral vasculature and blood flow as determined by quantitative optical coherence tomography angiography. Neurobiol Aging. 2018;70:148-59. doi:10.1016/j.neurobiolaging.2018.06.017
62. Montagne A, Barnes SR, Sweeney MD, Halliday MR, Sagare AP, Zhao Z, et al. Blood-brain barrier breakdown in the aging human hippocampus. Neuron. 2015;85(2):296-302. doi:10.1016/j.neuron.2014.12.032
63. Yu D, Mei Y, Wang L, Zhao Y, Fan X, Liang D, et al. Nano-seq analysis reveals different functional tendency between exosomes and microvesicles derived from hUMSC. Stem Cell Res Ther. 2023;14(1):272. doi:10.1186/s13287-023-03491-5
64. Abbas M, Jesel L, Auger C, Amoura L, Messas N, Manin G, et al. Endothelial microparticles from acute coronary syndrome patients induce premature coronary artery endothelial cell aging and thrombogenicity: role of the Ang II/AT1 receptor/NADPH oxidase-mediated activation of MAPKs and PI3-kinase pathways. Circulation. 2017;135(3):280-96. doi:10.1161/CIRCULATIONAHA.116.017513
65. Lin X, Li S, Wang YJ, Wang Y, Zhong JY, He JY, et al. Exosomal Notch3 from high glucose-stimulated endothelial cells regulates vascular smooth muscle cells calcification/aging. Life Sci. 2019;232:116582. doi:10.1016/j.lfs.2019.116582
66. Chen RW, Liu H, An JX, Qian XY, Jiang YD, Cope DK, et al. Cognitive effects of electro-acupuncture and pregabalin in a trigeminal neuralgia rat model induced by cobra venom. J Pain Res. 2017;10:1887-97. doi:10.2147/JPR.S140840
67. Taşdemir Ş, Morçimen ZG, Doğan AA, Görgün C, Şendemir A. Surface area of graphene governs its neurotoxicity. ACS Biomater Sci Eng. 2023;9(6):3297-305. doi:10.1021/acsbiomaterials.3c00104
68. Katsimpardi L, Litterman NK, Schein PA, Miller CM, Loffredo FS, Wojtkiewicz GR, et al. Vascular and neurogenic rejuvenation of the aging mouse brain by young systemic factors. Science. 2014;344(6184):630-4. doi:10.1126/science.1251141
69. Grillari J, Hackl M, Grillari-Voglauer R. miR-17-92 cluster: ups and downs in cancer and aging. Biogerontology. 2010;11(4):501-6. doi:10.1007/s10522-010-9272-9

70. Hu G, Xia Y, Zhang J, Chen Y, Yuan J, Niu X, et al. ESC-sEVs rejuvenate senescent hippocampal NSCs by activating lysosomes to improve cognitive dysfunction in vascular dementia. Adv Sci (Weinh). 2020;7(10):1903330. doi:10.1002/advs.201903330
71. Li G, Luna C, Qiu J, Epstein DL, Gonzalez P. Alterations in microRNA expression in stress-induced cellular senescence. Mech Ageing Dev. 2009;130(11-12):731-41. doi:10.1016/j.mad.2009.09.002
72. Chen Z, Pan X, Sheng Z, Yan G, Chen L, Ma G. miR-17 regulates the proliferation and apoptosis of endothelial cells in coronary heart disease via targeting insulin-like-growth factor 1. Pathol Res Pract. 2019;215(9):152512. doi:10.1016/j.prp.2019.152512
73. Hu Y, Bi Y, Yao D, Wang P, Li Y. Omi/HtrA2 protease associated cell apoptosis participates in blood-brain barrier dysfunction. Front Mol Neurosci. 2019;12:48. doi:10.3389/fnmol.2019.00048
74. Pan Q, Zheng J, Du D, Liao X, Ma C, Yang Y, et al. MicroRNA-126 priming enhances functions of endothelial progenitor cells under physiological and hypoxic conditions and their therapeutic efficacy in cerebral ischemic damage. Stem Cells Int. 2018;2018:2912347. doi:10.1155/2018/2912347
75. Montellano FA, Ungethüm K, Ramiro L, Nacu A, Hellwig S, Fluri F, et al. Role of blood-based biomarkers in ischemic stroke prognosis: a systematic review. Stroke. 2021;52(2):543-51. doi:10.1161/STROKEAHA.120.029232
76. Kuracha MR, Thomas P, Tobi M, McVicker BL. Role of cell-free network communication in alcohol-associated disorders and liver metastasis. World J Gastroenterol. 2021;27(41):7080-99. doi:10.3748/wjg.v27.i41.7080
77. Wise PM, Sahana J, Neviani P, Corydon TJ, Schulz H, Wehland M, et al. Prolonged exposure to simulated microgravity changes release of small extracellular vesicle in breast cancer cells. Int J Mol Sci. 2022;23(24):16095. doi:10.3390/ijms232416095